

Classification: Biological Sciences; Neuroscience

Title: Diazepam Accelerates GABA_AR Synaptic Exchange and Alters Intracellular Trafficking

Authors: Joshua M. Lorenz-Guertin¹; Matthew J. Bambino¹; Sabyasachi Das¹; Susan T. Weintraub²; Tija C. Jacob¹

Affiliations:

Department of Pharmacology and Chemical Biology, University of Pittsburgh School of Medicine, Pittsburgh, PA 15261, USA¹

Department of Biochemistry & Structural Biology, UT Health Science Center at San Antonio, San Antonio, TX²

Corresponding Author: Tija C. Jacob

Phone Number: 412-648-8136

Email: tcj11@pitt.edu

Address: W1351 Thomas E. Starzl Biomedical Science Tower 200 Lothrop St., Pittsburgh, PA 15261

Abstract Despite 50+ years of clinical use as anxiolytics, anti-convulsants, and sedative/hypnotic agents, the mechanisms underlying benzodiazepine (BZD) tolerance are poorly understood. BZDs potentiate the actions of gamma-aminobutyric acid (GABA), the primary inhibitory neurotransmitter in the adult brain, through positive allosteric modulation of $\gamma 2$ subunit containing GABA type A receptors (GABA_ARs). Here we define key molecular events impacting $\gamma 2$ GABA_AR and the inhibitory synapse gephyrin scaffold following initial sustained BZD exposure in vitro and in vivo. Using immunofluorescence and biochemical experiments, we found that cultured cortical neurons treated with the classical BZD, diazepam (DZP), presented no substantial change in surface or synaptic levels of $\gamma 2$ -GABA_ARs. In contrast, both $\gamma 2$ and the postsynaptic scaffolding protein gephyrin showed diminished total protein levels following a single DZP treatment in vitro and in mouse cortical tissue. We further identified DZP treatment enhanced phosphorylation of gephyrin Ser270 and increased generation of gephyrin cleavage products. Selective immunoprecipitation of $\gamma 2$ from cultured neurons revealed enhanced ubiquitination of this subunit following DZP exposure. To assess novel trafficking responses induced by DZP, we employed a $\gamma 2$ subunit containing an N terminal fluorogen-activating peptide (FAP) and pH-sensitive green fluorescent protein ($\gamma 2^{\text{pH}}$ FAP). Live-imaging experiments using $\gamma 2^{\text{pH}}$ FAP GABA_AR expressing neurons identified enhanced lysosomal targeting of surface GABA_ARs and increased overall accumulation in vesicular compartments in response to DZP. Using fluorescence resonance energy transfer (FRET) measurements between $\alpha 2$ and $\gamma 2$ subunits within a GABA_AR in neurons, we identified reductions in synaptic clusters of this subpopulation of surface BZD sensitive receptor. Moreover, we found DZP simultaneously enhanced synaptic exchange of both $\gamma 2$ -GABA_ARs and gephyrin using fluorescence recovery after photobleaching (FRAP) techniques. Finally we provide the first proteomic analysis of the BZD sensitive GABA_AR interactome in DZP vs. vehicle treated mice. Collectively, our results indicate DZP exposure elicits down-regulation of gephyrin scaffolding and BZD sensitive GABA_AR synaptic availability via multiple dynamic trafficking processes.

Introduction

GABA_ARs are ligand-gated ionotropic chloride (Cl⁻) channels responsible for the majority of fast inhibitory neurotransmission in the adult CNS. The most prevalent synaptic GABA_AR subtype is composed of two α , two β , and a $\gamma 2$ subunit forming a heteropentamer (1). Benzodiazepines (BZD) are a widely used clinical sedative-hypnotic drug class that selectively binds between the interface of a $\gamma 2$ subunit and either an $\alpha 1/2/3/5$ subunit (2). Receptors containing these α subunits are considered to be primarily synaptic, with the exception of $\alpha 5$, which is localized both synaptically and extrasynaptically (3). Positive allosteric modulation by BZD enhances GABA_AR inhibition by increasing the binding affinity of GABA and increasing channel opening frequency (1). This potentiating effect of BZD is lost after prolonged or high dose acute exposure (4, 5), characterized first by a loss of sedative/hypnotic activity followed by the anti-convulsant properties behaviorally (6-9). The induction of BZD tolerance occurs in part due to the uncoupling of allosteric actions between GABA and BZD (10, 11), a process that appears to rely on GABA_AR receptor internalization (12, 13). We have previously shown that 24 h BZD treatment leads to decreased surface and total levels of the $\alpha 2$ subunit in cultured hippocampal neurons that was dependent on lysosomal-mediated degradation (14); however, the process by which the $\alpha 2$ subunit is selectively targeted to lysosomes is still unknown. GABA_AR subunit ubiquitination and subsequent degradation at proteasomes or lysosomes modulates cell surface

expression of receptors (15-19). Ubiquitination of the $\gamma 2$ subunit is the only currently known mechanism shown to target internalized surface GABA_ARs to lysosomes (16).

Another major regulator of GABA_AR efficacy is postsynaptic scaffolding. Confinement at synaptic sites maintains receptors at GABA axonal release sites for activation. Furthermore, this limits receptor diffusion into the extrasynaptic space where internalization occurs (20, 21). The scaffolding protein gephyrin is the main organizer of GABA_AR synaptic localization and density, as gephyrin knock-down and knock-out models show dramatic reductions in $\gamma 2$ - and $\alpha 2$ -GABA_AR clustering (22, 23). Evidence suggests gephyrin interacts directly with GABA_AR $\alpha 1$, $\alpha 2$, $\alpha 3$, $\alpha 5$, $\beta 2$, and $\beta 3$ subunits (3, 24, 25). Gephyrin recruitment is involved in inhibitory long term potentiation (26, 27), while its dispersal coincides with GABA_AR diffusion away from synapses (22, 28). Extensive post-translational modifications influence gephyrin function (29, 30). Accordingly, expression of gephyrin phosphorylation site mutants revealed complex effects on GABA_AR diffusion and gephyrin ultrastructure and scaffolding (30, 31). Phosphorylation at the gephyrin serine 270 (Ser270) site has been particularly characterized to negatively modulate scaffold clustering and density, in part by enhancing calpain-1 protease mediated degradation of gephyrin (32). Given the well-established interdependent relationship between gephyrin and the $\gamma 2$ subunit in maintaining receptor synaptic integrity (22, 23, 33-36), impaired postsynaptic scaffolding should affect both pre-existing and newly inserted GABA_AR clustering and ultimately the efficacy of inhibitory neurotransmission. Thus a central unanswered question is if BZD exposure causes changes in gephyrin phosphorylation or protein levels.

Here we demonstrate that 12-24 h treatment with the BZD, diazepam (DZP), leads to a reduction in total $\gamma 2$ subunit and gephyrin levels in vitro and in vivo. This reduction occurred coincident with enhanced $\gamma 2$ subunit ubiquitination, but resulted in no significant change in overall $\gamma 2$ surface levels. Using our recently published dual fluorescent BZD-sensitive GABA_AR reporter ($\gamma 2^{\text{PH}}\text{FAP}$), we further show that cell surface $\gamma 2$ -GABA_ARs are more frequently targeted to lysosomes after DZP exposure. Forester resonance energy transfer (FRET) experiments further confirmed specific loss of synaptic $\alpha 2/\gamma 2$ GABA_AR levels following DZP. The scaffolding protein gephyrin also demonstrated augmented phosphorylation at Ser270, increased cleavage and was significantly decreased in membrane and cytosolic compartments. Fluorescence recovery after photobleaching (FRAP) assays identified that DZP treatment increased the simultaneous recovery of $\gamma 2$ -GABA_AR and gephyrin at synaptic sites, indicating reduced receptor confinement and accelerated exchange between the synaptic and extrasynaptic GABA_AR pool. This process could be reversed by the BZD site antagonist Ro 15-1788. Lastly, coimmunoprecipitation, quantitative mass spectrometry and bioinformatics analysis revealed shifts in the $\gamma 2$ -GABA_AR interactome towards trafficking pathways in vivo. Together, these data suggest that DZP exposure causes compensatory decrease in inhibitory neurotransmission by reducing BZD-sensitive GABA_AR and gephyrin confinement at synapses, and via ubiquitination and lysosomal targeting of $\gamma 2$.

Results

DZP Exposure Modifies $\gamma 2$ -GABA_AR and Gephyrin Levels. We first examined if DZP exposure reduced surface levels of $\gamma 2$ -GABA_ARs and altered gephyrin S270 phosphorylation in cortical neurons by immunofluorescence (Fig. 1A). Cortical neurons were treated for 24 h with vehicle or 1 μM DZP, then immunostained for surface $\gamma 2$, followed by permeabilization and immunostaining with GAD65 (glutamic acid decarboxylase 65, a marker for presynaptic

GABAergic terminals) and the phospho-S270 specific gephyrin mAb7a antibody (37, 38). Image analysis identified no sizable change in surface synaptic ($91.6 \pm 5.3\%$) or extrasynaptic ($93.3 \pm 3.8\%$) $\gamma 2$ intensity in DZP treated neurons relative to control, but DZP induced a significant $18.9 \pm 7.4\%$ increase in synaptic phospho-gephyrin (Fig. 1B). No change in extrasynaptic phosphorylated Ser270 gephyrin was measured. We repeated this DZP treatment and examined total and phospho-gephyrin levels in dendrites (Fig. 1C). Again DZP significantly enhanced phospho-S270 gephyrin compared to vehicle ($132 \pm 12\%$), while a decrease in overall gephyrin levels was found ($69.7 \pm 5.4\%$) (Fig. 1D). Accordingly, the mean ratio of phospho/total gephyrin was $78.1 \pm 21\%$ higher following DZP (Fig. 1D). Complimentary biochemical studies using membrane fractionation were used to compare cytosolic, membrane, and total protein pools in cortical neurons. In agreement with immunofluorescence data, membrane levels of $\gamma 2$ ($97.1 \pm 10.2\%$) were not reduced after $1 \mu\text{M}$ DZP, although the total pool of $\gamma 2$ was diminished ($79.3 \pm 7.3\%$) (Fig. 2A,B) compared to vehicle. Comparatively, DZP reduced gephyrin in every compartment measured relative to control (cytosol: $87.3 \pm 4.6\%$; membrane: $70.3 \pm 10\%$; total: $59.1 \pm 3.4\%$). We confirmed the integrity of our fractions using cytosolic and membrane specific markers (Supplemental Fig. 1).

Next we assessed if the decrease in gephyrin and $\gamma 2$ total levels at 24 hours was a result of altered gene expression. qRT-PCR experiments revealed no difference in gephyrin, $\gamma 2$, or control GABA_AR $\beta 3$ subunit mRNA levels between vehicle and DZP treated neurons (Fig. 2C). To determine if post-translational modification of $\gamma 2$ also occurs coincident with decreased $\gamma 2$ protein levels, we examined ubiquitination of $\gamma 2$ in response to DZP exposure. We reasoned that changes in ubiquitination of $\gamma 2$ would likely precede the loss of total $\gamma 2$ seen at 24 h (Fig. 2A,B). GFP-ubiquitin transfected cortical neurons were treated with vehicle or $1 \mu\text{M}$ DZP for 12 h. Neurons were lysed under denaturing conditions to isolate the $\gamma 2$ subunit from the receptor complex (Supplemental Fig. 2). Immunoprecipitation of the $\gamma 2$ subunit revealed a 2.13 fold increase in ubiquitination in DZP treated neurons relative to vehicle (Fig. 2D,E). Furthermore, just as observed with 24 h DZP treatment, a reduced total pool of $\gamma 2$ was also found at 12 h (Fig. 2D,E). Notably, this is the first demonstration of endogenous $\gamma 2$ ubiquitination occurring in neurons (previous findings were of recombinant receptors in HEK cells) (15, 16). To investigate mechanisms underlying reduced gephyrin levels, we examined gephyrin cleavage. Gephyrin is degraded post-translationally by the protease calpain-1 (32, 39, 40), and gephyrin Ser270 phosphorylation promotes cleavage by calpain-1 (32). Consistent with the enhanced gephyrin S270 phosphorylation (Fig. 1) and reduced total levels (Fig. 1,2) we found a significant increase in the ratio of cleaved/full length gephyrin after 24 h DZP in vitro (Fig. 2F,G). We confirmed the identity of the gephyrin cleavage product using a well-characterized glutamate stimulation protocol that induces gephyrin cleavage in cultured neurons (39, 40), a process blocked by calpain-1 inhibition (Supplemental Fig. 3).

Finally, we wanted to determine if similar mechanisms occur in vivo following DZP treatment. Prior publications show that BZDs and metabolites are not present 24 h post-injection due to rapid drug metabolism in rodents (41-44). Furthermore, BZD uncoupling does not persist 24 h after a single dose (15 mg/kg) or 2 week daily DZP treatment, whereas uncoupling can be seen 12 h after a single injection, indicating this is the appropriate timepoint for measuring in vivo loss of $\gamma 2$ -GABA_AR function (4). Accordingly, mice were given a single intraperitoneal (IP) injection of 10 mg/kg DZP or vehicle control, and cortex tissues were harvested 12 h later. We found DZP significantly reduced the total pool of $\gamma 2$ ($87.3 \pm 3.0\%$) and gephyrin ($73.9 \pm 9.1\%$) relative to vehicle treated mice at 12 h post injection (Fig. 2H,I). These findings indicate both

BZD-sensitive GABA_ARs and gephyrin are downregulated by post-translational mechanisms after initial DZP treatment in vitro and in vivo to temper potentiation of GABA_AR function.

DZP Enhances Intracellular Accumulation and Lysosomal Targeting of $\gamma 2$ -GABA_ARs. We then investigated if surface DZP-sensitive GABA_ARs are more frequently targeted to lysosomes after DZP exposure by live-imaging. For these experiments we used our recently characterized optical sensor for synaptic GABA_AR ($\gamma 2^{\text{pH}}$ FAP). This dual reporter is composed of a $\gamma 2$ subunit tagged with an N terminal pH-sensitive GFP, myc, and the fluorogen-activating peptide DL5 (45). The pH-sensitive GFP tag selectively identifies cell surface GABA_ARs and the DL5 FAP binds malachite green (MG) dye derivatives including MG-BTau (46-48). MG-BTau is cell impermeable and non-fluorescent until bound by DL5. Upon binding, MG-BTau fluoresces in the far red spectral region (~670 nm). This FAP-dye system allows for selective labeling of surface $\gamma 2$ -containing GABA_ARs which can then be tracked through various phases of trafficking (45). As previously shown, $\gamma 2^{\text{pH}}$ FAP GABA_ARs are expressed on the neuronal surface, form synaptic clusters, do not perturb neuronal development and show equivalent functional responsiveness to GABA and DZP both in the absence and presence of MG dyes (45). We transfected neurons with $\gamma 2^{\text{pH}}$ FAP and treated them with DZP for 8-16 h. Neurons were then pulse-labeled with 100 nM MG-BTau dye and returned to conditioned media at 37°C +/- DZP for 1 h. The lysosomal inhibitor leupeptin (200 μ M) and the lysosomal specific dye, LysoTracker (50 nM), were added after 30 min. At the end of the incubation, neurons were washed in 4°C saline to inhibit trafficking and immediately used for live-imaging experiments. Representative images demonstrate MG-BTau labeled $\gamma 2^{\text{pH}}$ FAP-GABA_ARs localized on the cell surface (Fig. 3A) and at synaptic clusters on dendrites (Fig. 3B) based on colocalization with surface specific pHGFP signal. MG-BTau further reveals internalized receptors at lysosomes (Fig. 3C). Image quantification showed synaptic $\gamma 2$ -GABA_AR intensity remained largely unchanged (Fig. 3D). Importantly, we found a significant $8.0 \pm 2.5\%$ enhancement in the mean intensity of GABA_ARs labeled with MG-BTau at lysosomes following DZP (Fig. 3E).

We complemented these lysosomal targeting studies with an NH₄Cl live-imaging approach that allows us to compare the ratio of cell surface vs. intracellular GABA_ARs in living neurons. $\gamma 2^{\text{pH}}$ FAP expressing neurons were treated with vehicle or DZP for 24 h. Additional control groups included the BZD antagonist Ro 15-1788 (1-2 h) to reverse the effects of DZP. Neurons were actively perfused with HEPES buffered saline (HBS) treatment and an initial image was taken of surface pHGFP receptor signal (Fig. 3F). Neurons were then exposed to pH 7.4 NH₄Cl solution to neutralize the pH gradient of all intracellular membrane compartments, revealing internal pools of $\gamma 2$ containing GABA_ARs. Analysis revealed no change in surface $\gamma 2$ levels between treatments (Fig. 3G) consistent with (Fig. 1, 2). However, the number of large intracellular vesicles (circular area ~0.75 μ m) containing receptors was significantly enhanced (Fig. 3H), consistent with increased localization in intracellular vesicles. Ro 15-1788 and DZP + Ro 15-1788 treated neurons were not significantly different from vehicle. Overall, these findings suggest $\gamma 2$ -GABA_AR ubiquitination, intracellular accumulation, lysosomal targeting and degradation are part of the adaptive response to DZP.

Surface Levels of Synaptic $\alpha 2/\gamma 2$ GABA_AR are Decreased Following DZP. Despite the increase in ubiquitination and lysosomal targeting of $\gamma 2$ -GABA_ARs after DZP, we did not detect decreased overall surface or synaptically localized surface $\gamma 2$ levels. This suggested two possibilities, one being that as DZP treatment only reduced total $\gamma 2$ levels to 80% of control in

cortical neurons and 85% in vivo, such a slight decrease in surface $\gamma 2$ -GABA_ARs would be challenging to detect with current methods. Alternatively, there could be an increase in $\gamma 2$ subunit assembly with BZD-insensitive α subunits ($\gamma 2\alpha 4\beta$) (49) with a concomitant reduction in surface levels of BZD-sensitive receptors ($\gamma 2\alpha 1/2/3/5\beta$). Our previous work showed 24 h BZD exposure in hippocampal neurons causes decreased total and surface levels of the $\alpha 2$ GABA_AR subunit via lysosomal mediated degradation, without any changes in receptor insertion or removal rate (14). To determine if $\alpha 2/\gamma 2$ GABA_ARs are specifically decreased by DZP treatment, we developed and employed an intermolecular FRET assay, using pH-sensitive GFP tagged $\alpha 2^{\text{pH}}$ (50) as a donor fluorophore and a red fluorescent protein (RFP) tagged $\gamma 2$ subunit ($\gamma 2^{\text{RFP}}$) as an acceptor. FRET is an accurate measurement of molecular proximity at distances of 10-100 Å and is highly efficient if donor and acceptor are within the Förster radius, typically 30-60 Å (3-6 nM), with the efficiency of FRET being dependent on the inverse sixth power of intermolecular separation (51). Synaptic GABA_ARs exist as five subunits assembled in $\gamma 2$ - α - β - α - β order forming a heteropentameric ion channel (Fig. 4A). We first expressed $\alpha 2^{\text{pH}}$ and $\gamma 2^{\text{RFP}}$ in neurons and examined their ability to participate in intermolecular FRET. Photobleaching of the acceptor $\gamma 2^{\text{RFP}}$ channel enhanced donor $\alpha 2^{\text{pH}}$ signal (Supplementary Fig. 4), confirming energy transfer from $\alpha 2^{\text{pH}}$ to $\gamma 2^{\text{RFP}}$. Next, we confirmed measurable FRET only occurs between $\alpha 2^{\text{pH}}/\gamma 2^{\text{RFP}}$ in surface GABA_AR at synaptic sites; FRET was blocked with quenching of donor $\alpha 2^{\text{pH}}$ when the extracellular pH was reduced from 7.4 to 6.0 (Fig. 4A,B). Following FRET assay validation, $\alpha 2^{\text{pH}}/\gamma 2^{\text{RFP}}$ GABA_AR expressing neurons were treated for 24 h with vehicle or DZP and examined for total synaptic $\alpha 2^{\text{pH}}$ and $\gamma 2^{\text{RFP}}$ fluorescence as well as the $\gamma 2$ FRET signal (Fig. 4A). These studies identified a DZP-induced reduction in synaptic $\alpha 2$ (-12.6%), synaptic $\gamma 2$ (-14.3%) and diminished association of $\alpha 2$ with $\gamma 2$ in synaptic GABA_ARs as measured by decreased FRET $\gamma 2$ signal (-10.6%) (Fig. 4B). In summary, this sensitive FRET method indicates that cortical neurons show a similar susceptibility for $\alpha 2$ subunit downregulation by BZD treatment as seen in hippocampal neurons (14). Furthermore it identifies a loss in a specific pool of surface synaptic BZD-sensitive $\gamma 2$ -GABA_AR.

Synaptic Exchange of $\gamma 2$ -GABA_ARs and Gephyrin are Accelerated after Prolonged DZP Treatment. We previously found 24 h BZD exposure reduces the amplitude of miniature inhibitory postsynaptic currents (mIPSC) (14), suggesting changes in synaptic GABA_AR function. Having identified both reductions in gephyrin (Fig. 1,2) and BZD sensitive GABA_ARs (Fig. 2, 4), we next tested if DZP treatment altered the synaptic retention properties of gephyrin and/or GABA_ARs. Neurons expressing $\gamma 2^{\text{pH}}$ FAP and RFP-gephyrin were used for live-imaging fluorescence recovery after photobleaching experiments (FRAP) to measure synaptic and extrasynaptic exchange following exposure to vehicle, 1 μM DZP, 5 μM Ro 15-1788, or DZP + Ro 15-1788. After an initial image was taken, dendrites were photobleached, and signal recovery was measured every 2 min over 30 min at synaptic sites and extrasynaptic regions (Fig. 5A synapses panel; Fig. 5B larger dendritic region with asterisk denoting extrasynaptic region). MG-BTau dye was added directly after the photobleaching step to immediately re-identify the photobleached surface synaptic GABA_ARs, and improve spatial measurements (Fig. 5B). These experiments revealed synaptic $\gamma 2$ turnover rates were nearly doubled in DZP treated neurons, a process reversed by Ro 15-1788 co-treatment (Fig. 5C). DZP also accelerated gephyrin synaptic exchange rates compared to vehicle, with Ro 15-1788 co-treatment restoring exchange to control levels. No significant correlation was found between cluster area measured and fluorescence recovery rates of $\gamma 2$ and gephyrin across all conditions, suggesting synaptic exchange rate is

independent of cluster size (Supplementary Fig. 5). Moreover, no statistical difference was found in $\gamma 2$ or gephyrin extrasynaptic exchange rates (Fig. 5D). These findings suggest concurrent reduction of gephyrin and GABA_AR synaptic confinement is a compensatory response to mitigate prolonged DZP potentiation of GABA_ARs.

Coimmunoprecipitation and Quantitative Proteomics of $\gamma 2$ GABA_AR following DZP injection. We sought to observe DZP-induced changes in receptor trafficking in vivo. As an orthogonal approach, we utilized label-free quantitative proteomics to measure changes in the quantities of proteins associated with $\gamma 2$ -GABA_ARs in the cortex of mice after DZP. Cortical tissue was collected from DZP- or vehicle-treated mice 12 h post injection, lysed, and immunoprecipitated with anti- $\gamma 2$ subunit antibody or IgG control. Following label-free mass spectrometry analysis, spectrum counts were used to assess relative abundance of $\gamma 2$ -associated proteins. A total of 395 proteins was identified using our inclusion criteria: minimum of two peptides; identified in at least three samples overall or in two of three samples in a specific treatment group; demonstrated at least 3:1 enrichment over IgG control across at least three samples overall (Dataset 1). The relative abundance of $\gamma 2$ -GABA_AR associated proteins in the DZP group compared to vehicle was used to determine which proteins were significantly ($P < 0.1$) increased (Table 1) or decreased (Table 2). As a result we identified 46 proteins with elevated levels of interaction with $\gamma 2$ -GABA_ARs, including 10 proteins that were only found in the DZP treated group (Table 1, not found in vehicle samples, NF-V). Increased interactions were shown for 14-3-3 epsilon. In contrast, 23 proteins were found to coimmunoprecipitate with $\gamma 2$ less in DZP animals relative to control, seven of which were only present in the vehicle treatment group (Table 2, not found in DZP, NF-DZP). Interestingly, the calcium-sensitive kinase CaMKII α , which can regulate GABA_AR membrane insertion, synaptic retention and drug binding properties (26, 70-72), was found to be significantly decreased in interaction with $\gamma 2$ -GABA_AR following DZP injection in vivo.

Bioinformatics Analysis of the $\gamma 2$ GABA_AR interactome. To better understand the consequences of the DZP-induced shift in the $\gamma 2$ -GABA_AR protein interaction network, protein fold change data was subjected to core Ingenuity Pathway Analysis (IPA). Top enriched canonical pathways with $-\log(p\text{-value}) > 6.2$ are shown in Fig. 6A. Notably, GABA receptor signaling pathways were highly enriched, as expected, although IPA was unable to determine pathway activation status by z-score analysis. $\gamma 2$ -GABA_AR association with proteins involved in 14-3-3 mediated signaling and RhoA signaling pathways were greatly increased after DZP (Fig. 6A, orange), while interaction with proteins involved in EIF2 signaling and sirtuin signaling pathways were reduced (Fig. 6A, blue) relative to vehicle.

We further examined alterations in functional network association, identifying changes in key trafficking, localization, and cell adhesion pathways in DZP treated mice. Fig. 6B lists $\gamma 2$ -GABA_AR-associated proteins found to be elevated with DZP, contributing to processes such as endocytosis, developmental process of the synapse, cell-cell contact, and quantity of cell-cell contacts (activation z-scores > 2.5). As an additional measurement, we performed gene ontology (GO) database analysis of proteins which were found to be significantly increased ($P < 0.1$) in DZP treated mice relative to vehicle control (Table 3). GO analysis identified DZP treatment enriched for a number of intracellular trafficking and cellular localization biological pathways that were consistent with the functional network analysis in IPA. Taken together, these results suggest DZP modifies intracellular and surface trafficking of $\gamma 2$ -GABA_ARs both in vitro and in vivo.

Discussion

This work identifies key trafficking pathways involved in GABA_AR neuroplasticity in response to initial DZP exposure. Using a combination of biochemical and imaging techniques, we identified total $\gamma 2$ subunit levels are diminished in response to 12-24 h of DZP exposure in vitro and in vivo. Concurrent with the decrease in the overall $\gamma 2$ pool, we found DZP treatment enhanced ubiquitination of this subunit. Use of an innovative optical sensor for BZD sensitive GABA_AR ($\gamma 2^{\text{pH}}$ FAP) in combination with MG dye pulse-labeling approaches revealed DZP exposure moderately enhanced targeting of surface $\gamma 2$ -GABA_ARs to lysosomes. Live-imaging experiments with pH 7.4 NH₄Cl revealed increased intracellular receptor pools, providing further evidence that DZP enhances GABA_AR lysosomal accumulation, a response reversed by BZD antagonist Ro 15-1788 treatment. We used novel intersubunit FRET based live-imaging to identify that surface synaptic $\alpha 2/\gamma 2$ GABA_ARs were specifically decreased after DZP, suggesting these receptor complexes were subjected to ubiquitination, lysosomal targeting, and degradation. In addition to DZP modulation of receptor trafficking, the postsynaptic scaffolding protein gephyrin demonstrated significant plasticity including increased Ser270 phosphorylation and production of gephyrin proteolytic fragments, concurrent with a decrease in total and membrane associated gephyrin levels. Given the fundamental role of gephyrin in scaffolding GABA_ARs and regulating synaptic confinement, we used simultaneous FRAP live-imaging of receptors and scaffold in neurons to monitor inhibitory synaptic dynamics. We found ~24 h DZP exposure accelerates both the rate of gephyrin and GABA_AR exchange at synapses as shown by enhanced fluorescence recovery rates. Control experiments using the BZD antagonist Ro 15-1788 were able to reverse the DZP induced loss of synaptic confinement, reducing gephyrin and GABA_AR mobility back to vehicle levels. Finally, we used label-free quantitative mass spectrometry and bioinformatics to identify key changes in $\gamma 2$ -GABA_AR protein association in vivo suggesting enhanced accumulation in cell surface and intracellular trafficking networks. Collectively, this work defines a DZP-induced reduction of gephyrin scaffolding coupled with increased synaptic exchange of gephyrin and GABA_ARs. This dynamic flux of GABA_ARs between synapses and the extrasynaptic space was associated with enhanced $\gamma 2$ -GABA_AR accumulation in intracellular vesicles and $\gamma 2$ -GABA_AR subtype specific lysosomal degradation. We propose DZP treatment alters these key intracellular and surface trafficking pathways ultimately diminishing responsiveness to DZP.

Numerous classical studies have examined gene and protein expression adaptations in GABA_AR subunits after BZD exposure with minimal agreement that a specific change occurs (1, 2, 6). Here molecular mechanistic insight is provided, through direct measurements of enhanced ubiquitination of the $\gamma 2$ subunit (Fig. 2), lysosomal targeting (Fig. 3), reduced surface synaptic $\alpha 2/\gamma 2$ GABA_AR levels (Fig. 4), and reduced synaptic confinement (Fig. 5) of DZP-sensitive GABA_ARs. Together this suggests BZD exposure primarily decreases synaptic retention of $\gamma 2$ containing GABA_AR while downregulating surface levels of specific α subunit levels. Ubiquitination of the $\gamma 2$ subunit by the E3 ligase Ring Finger Protein 34 (RNF 34) (36) is the only currently known mechanism targeting internalized synaptic GABA_ARs to lysosomes (37). Due to the requirement of the $\gamma 2$ subunit in all BZD-sensitive GABA_ARs, it is likely that ubiquitination of the $\gamma 2$ subunit is a contributing factor for increased lysosomal-mediated degradation in response to DZP. Despite a small decrease in the $\gamma 2$ total protein, changes in surface levels were not significant by biochemical approaches, consistent with evidence that $\gamma 2$ -GABA_AR surface levels are tightly regulated to maintain baseline inhibition and prevent excitotoxicity. For example, in heterozygous $\gamma 2$ knockout mice a 50% reduction in $\gamma 2$ levels

appears to be compensated by increased cell surface trafficking, resulting in only approximately a 20% reduction in BZD binding sites in the cortex and a limited reduction in synaptic GABA_AR clusters. In contrast, homozygous $\gamma 2$ knockout mice show a complete loss of behavioral drug response to BZD and over 94% of the BZD sites in the brain (GABA binding sites unchanged) and early lethality (52). Similarly, studies have shown that prolonged GABA_AR agonist or BZD application increases $\gamma 2$ GABA_AR internalization in cultured neurons, while surface GABA_AR levels remain unchanged (53, 54). Importantly, by using high sensitivity surface GABA_AR intersubunit FRET measurements we were able to detect a decrease in BZD sensitive $\alpha 2/\gamma 2$ GABA_ARs (Fig 4).

The role of inhibitory scaffolding changes in responsiveness to BZD has been largely under investigated. Phosphorylation of gephyrin at Ser270 is mediated by CDK5 and GSK3 β , while a partnering and functionally relevant Ser268 site is regulated by ERK1/2 (31). While the exact signaling mechanism responsible for gephyrin remodeling and phosphorylation in our study is unclear, we have previously shown 30 min treatment with the GABA_AR agonist muscimol leads to ERK1/2/BDNF signaling, decreased gephyrin synaptic and total levels, and decreased $\gamma 2$ -GABA_AR at synapses and potentiation by BZDs (55). Thus, changes in receptor and scaffold synaptic level and function can occur on the timescale of minutes. Similarly, calpain mediated gephyrin cleavage can occur within 1 minute in hippocampal membranes (56), and cleavage products are increased following in vitro ischemia at 30 min and up to 48 hours following ischemic events in vivo (39). Additionally, chemically-induced inhibitory long-term potentiation (iLTP) protocols demonstrate gephyrin accumulation occurs concurrent with the synaptic recruitment of GABA_ARs within 20 min (26). Collectively, these proteins display a high degree of interdependence across different experimental paradigms of inhibitory synapse plasticity occurring over minutes to days.

A recent work has demonstrated 12 h DZP treatment of organotypic hippocampal slices expressing eGFP-gephyrin caused enhanced gephyrin mobility at synapses and reduced gephyrin cluster size (57). Here we found the synaptic exchange rate of $\gamma 2$ GABA_ARs and gephyrin to be nearly doubled at synapses in cortical neurons after ~24 h DZP exposure (Fig. 4). This effect occurred coincident with the formation of truncated gephyrin cleavage products (Fig. 2), which has previously been shown to decrease $\gamma 2$ synaptic levels (39). These findings are also consistent with our previous work showing RNAi gephyrin knockdown doubles the rate of $\gamma 2$ -GABA_AR turnover at synaptic sites (22). Later quantum dot single particle tracking studies confirmed $\gamma 2$ synaptic residency time is linked to gephyrin scaffolding levels (58). Importantly, GABA_AR diffusion dynamics also reciprocally regulate gephyrin scaffolding levels (59), suggesting gephyrin and GABA_ARs synaptic residency are often functionally coupled. Accordingly, $\gamma 2$ subunit and gephyrin levels both decrease in responses to other stimuli including status epilepticus (60) or prolonged inhibition of IP₃ receptor-dependent signaling (61).

Increasing receptor synaptic retention enhances synaptic currents, while enhanced receptor diffusion via decreased scaffold interactions reduces synaptic currents. For example, reduction of gephyrin binding by replacement of the $\alpha 1$ GABA_AR subunit gephyrin binding domain with non gephyrin binding homologous region of the $\alpha 6$ subunit results in faster receptor diffusion rates and a direct reduction in mIPSC amplitude (62). Similarly, enhanced diffusion of GABA_ARs following estradiol treatment also reduces mIPSCs in cultured neurons and in hippocampal slices (63). In contrast, brief DZP exposure (< 1h) reduces GABA_AR synaptic mobility (64) without a change in surface levels (65), consistent with initial synaptic potentiation of GABA_AR neurotransmission by DZP. Together with our current findings, this suggests post-

translational modifications on GABA_AR subunits or gephyrin that enhance receptor diffusion are a likely key step leading to functional tolerance to BZD drugs.

It is a significant technical challenge to examine dynamic alterations in receptor trafficking occurring in vivo. To overcome this we examined changes in γ 2-GABA_AR protein association following DZP injection in mice using quantitative proteomics and bioinformatics analysis. This work revealed shifts toward γ 2-GABA_AR association with new protein pathway networks associated with cell surface adhesion, intracellular junctions, synaptic plasticity, endocytosis & recycling and ubiquitination (Fig. 6, Table 3), confirming similar fluctuations in membrane and intracellular trafficking occur in vivo and in vitro after DZP. Recent inhibitory synapse proteomics studies have identified a number of new protein synaptic constituents or modulators of GABA_AR function (66-70). We show here that proteins known to have roles in synaptic function and trafficking of membrane receptors show changes in their association with γ 2- receptors. For example, the calcium-sensitive kinase CaMKII α was found to be significantly decreased in interaction with γ 2-GABA_AR following DZP, which can regulate GABA_AR membrane insertion, synaptic retention and drug binding properties (26, 71-73) (Table 2). DZP was also found to significantly increase γ 2 association with 14-3-3 protein family members (Table 1), which are known mediators of GABA_AR surface and intracellular trafficking (74, 75). γ 2 coassembly with the GABA_AR α 5 subunit was also enhanced after DZP (Table 1). Interestingly, the α 5 subunit is required for the development of BZD sedative tolerance in mice (76). Future follow up studies are needed to dissect the individual roles of proteins found to be significantly altered in their association with GABA_AR, and their physiological and pharmacological importance to BZD tolerance and inhibitory neurotransmission.

Through application of novel and highly sensitive fluorescence imaging approaches combined with in vivo proteomics, we provide unprecedented resolution at both the level of the single neuron and cortex of GABA_AR synapse plasticity induced by BZDs. Our study reveals that sustained initial DZP treatment diminishes synaptic BZD sensitive GABA_AR availability through multiple fundamental cellular mechanisms: through reduction of the post-synaptic scaffolding protein gephyrin; shifts toward intracellular trafficking pathways and targeting of receptors for lysosomal degradation; and enhanced synaptic exchange of both gephyrin and GABA_ARs. Proteomic and bioinformatics studies using DZP-treated mouse brain tissue provide further evidence that altered γ 2-GABA_AR surface and intracellular trafficking mechanisms play a critical role to the response to DZP in vivo. These results define key events leading to BZD irresponsiveness in initial sustained drug exposure. Future studies utilizing this dual approach will address the neuroadaptations produced by long term BZD use to systematically identify the effects of a critical drug class that has seen a tripling in prescription numbers over the last two decades (77).

Materials and Methods

Biochemical experiments, confocal imaging, image analysis. Detailed methods of cell culture, reagents, animals, imaging, biochemical protocols, mass spectrometry, bioinformatics and analysis are described in *SI Materials and Methods*.

ACKNOWLEDGEMENTS. This work was supported by funding from a National Institute of Health Training Grant (T32GM008424), National Institutes of Health Predoctoral Individual National Research Service Award (F31 MH117839), University of Pittsburgh Pharmacology and

Chemical Biology Fellowship (William C. deGroat Neuropharmacology Departmental Fellowship), NARSAD young investigator grant and Pharmacology and Chemical Biology Startup Funds. We thank Jonathan Beckel for technical advice on qRT-PCR and Katarina Vajn for assistance with neuronal cultures. Mass spectrometry analyses were conducted at the UTHSCSA Institutional Mass Spectrometry Laboratory, supported in part by UTHSCSA and the University of Texas System for purchase of the Orbitrap Fusion Lumos mass spectrometer. The expert technical assistance of Sammy Pardo and Dana Molleur is gratefully acknowledged.

1. Uusi-Oukari M & Korpi ER (2010) Regulation of GABA(A) receptor subunit expression by pharmacological agents. *Pharmacological reviews* 62(1):97-135.
2. Vinkers CH & Olivier B (2012) Mechanisms Underlying Tolerance after Long-Term Benzodiazepine Use: A Future for Subtype-Selective GABA(A) Receptor Modulators? *Advances in pharmacological sciences* 2012:416864.
3. Brady ML & Jacob TC (2015) Synaptic localization of alpha5 GABA (A) receptors via gephyrin interaction regulates dendritic outgrowth and spine maturation. *Developmental neurobiology* 75(11):1241-1251.
4. Holt RA, Bateson AN, & Martin IL (1999) Decreased GABA enhancement of benzodiazepine binding after a single dose of diazepam. *Journal of neurochemistry* 72(5):2219-2222.
5. Tietz EI, Chiu TH, & Rosenberg HC (1989) Regional GABA/benzodiazepine receptor/chloride channel coupling after acute and chronic benzodiazepine treatment. *European journal of pharmacology* 167(1):57-65.
6. Bateson AN (2002) Basic pharmacologic mechanisms involved in benzodiazepine tolerance and withdrawal. *Current pharmaceutical design* 8(1):5-21.
7. File SE, Wilks LJ, & Mabbitt PS (1988) Withdrawal, tolerance and sensitization after a single dose of lorazepam. *Pharmacology, biochemistry, and behavior* 31(4):937-940.
8. Wong PT, Yoong YL, & Gwee MC (1986) Acute tolerance to diazepam induced by benzodiazepines. *Clinical and experimental pharmacology & physiology* 13(1):1-8.
9. Lister RG & Nutt DJ (1986) Mice and rats are sensitized to the proconvulsant action of a benzodiazepine-receptor inverse agonist (FG 7142) following a single dose of lorazepam. *Brain research* 379(2):364-366.
10. Gallager DW, Lakoski JM, Gonsalves SF, & Rauch SL (1984) Chronic benzodiazepine treatment decreases postsynaptic GABA sensitivity. *Nature* 308:74.
11. Marley RJ & Gallager DW (1989) Chronic diazepam treatment produces regionally specific changes in GABA-stimulated chloride influx. *European journal of pharmacology* 159(3):217-223.
12. Gutierrez ML, Ferreri MC, & Gravielle MC (2014) GABA-induced uncoupling of GABA/benzodiazepine site interactions is mediated by increased GABAA receptor internalization and associated with a change in subunit composition. *Neuroscience* 257:119-129.
13. Ali NJ & Olsen RW (2001) Chronic benzodiazepine treatment of cells expressing recombinant GABA(A) receptors uncouples allosteric binding: studies on possible mechanisms. *Journal of neurochemistry* 79(5):1100-1108.
14. Jacob TC, *et al.* (2012) Benzodiazepine treatment induces subtype-specific changes in GABA(A) receptor trafficking and decreases synaptic inhibition. *Proceedings of the National Academy of Sciences of the United States of America* 109(45):18595-18600.
15. Jin H, *et al.* (2014) Ring finger protein 34 (RNF34) interacts with and promotes gamma-aminobutyric acid type-A receptor degradation via ubiquitination of the gamma2 subunit. *The Journal of biological chemistry* 289(42):29420-29436.

16. Arancibia-Carcamo IL, *et al.* (2009) Ubiquitin-dependent lysosomal targeting of GABA(A) receptors regulates neuronal inhibition. *Proceedings of the National Academy of Sciences of the United States of America* 106(41):17552-17557.
17. Di XJ, *et al.* (2016) Grp94 Protein Delivers gamma-Aminobutyric Acid Type A (GABAA) Receptors to Hrd1 Protein-mediated Endoplasmic Reticulum-associated Degradation. *The Journal of biological chemistry* 291(18):9526-9539.
18. Crider A, Pandya CD, Peter D, Ahmed AO, & Pillai A (2014) Ubiquitin-proteasome dependent degradation of GABAA α 1 in autism spectrum disorder. *Molecular autism* 5(1):1-10.
19. Saliba RS, Michels G, Jacob TC, Pangalos MN, & Moss SJ (2007) Activity-dependent ubiquitination of GABA(A) receptors regulates their accumulation at synaptic sites. *The Journal of neuroscience : the official journal of the Society for Neuroscience* 27(48):13341-13351.
20. Bogdanov Y, *et al.* (2006) Synaptic GABAA receptors are directly recruited from their extrasynaptic counterparts. *The EMBO journal* 25(18):4381-4389.
21. Gu Y, *et al.* (2016) Differential vesicular sorting of AMPA and GABAA receptors. *Proceedings of the National Academy of Sciences of the United States of America* 113(7):E922-931.
22. Jacob TC, *et al.* (2005) Gephyrin regulates the cell surface dynamics of synaptic GABAA receptors. *The Journal of neuroscience : the official journal of the Society for Neuroscience* 25(45):10469-10478.
23. Kneussel M, *et al.* (1999) Loss of postsynaptic GABA(A) receptor clustering in gephyrin-deficient mice. *The Journal of neuroscience : the official journal of the Society for Neuroscience* 19(21):9289-9297.
24. Tyagarajan SK & Fritschy JM (2014) Gephyrin: a master regulator of neuronal function? *Nature reviews. Neuroscience* 15(3):141-156.
25. Kowalczyk S, *et al.* (2013) Direct binding of GABAA receptor beta2 and beta3 subunits to gephyrin. *The European journal of neuroscience* 37(4):544-554.
26. Petrini EM, *et al.* (2014) Synaptic recruitment of gephyrin regulates surface GABAA receptor dynamics for the expression of inhibitory LTP. *Nature communications* 5:3921.
27. Flores CE, *et al.* (2015) Activity-dependent inhibitory synapse remodeling through gephyrin phosphorylation. *Proceedings of the National Academy of Sciences of the United States of America* 112(1):E65-72.
28. Bannai H, *et al.* (2009) Activity-dependent tuning of inhibitory neurotransmission based on GABAAR diffusion dynamics. *Neuron* 62(5):670-682.
29. Zacchi P, Antonelli R, & Cherubini E (2014) Gephyrin phosphorylation in the functional organization and plasticity of GABAergic synapses. *Frontiers in cellular neuroscience* 8:103.
30. Ghosh H, *et al.* (2016) Several posttranslational modifications act in concert to regulate gephyrin scaffolding and GABAergic transmission. *Nat Commun* 7:13365.
31. Battaglia S, Renner M, Rousseau M, & Come E (2018) Activity-Dependent Inhibitory Synapse Scaling Is Determined by Gephyrin Phosphorylation and Subsequent Regulation of GABAA Receptor Diffusion. 5(1).
32. Tyagarajan SK, *et al.* (2013) Extracellular signal-regulated kinase and glycogen synthase kinase 3 β regulate gephyrin postsynaptic aggregation and GABAergic synaptic function in a calpain-dependent mechanism. *J Biol Chem* 288(14):9634-9647.
33. Essrich C, Lorez M, Benson JA, Fritschy JM, & Luscher B (1998) Postsynaptic clustering of major GABAA receptor subtypes requires the gamma 2 subunit and gephyrin. *Nature neuroscience* 1(7):563-571.
34. Schweizer C, *et al.* (2003) The gamma 2 subunit of GABA(A) receptors is required for maintenance of receptors at mature synapses. *Molecular and cellular neurosciences* 24(2):442-450.
35. Alldred MJ, Mulder-Rosi J, Lingenfelter SE, Chen G, & Luscher B (2005) Distinct gamma2 subunit domains mediate clustering and synaptic function of postsynaptic GABAA receptors and

- gephyrin. *The Journal of neuroscience : the official journal of the Society for Neuroscience* 25(3):594-603.
36. Li RW, *et al.* (2005) Disruption of postsynaptic GABA receptor clusters leads to decreased GABAergic innervation of pyramidal neurons. *Journal of neurochemistry* 95(3):756-770.
37. Kuhse J, *et al.* (2012) Phosphorylation of gephyrin in hippocampal neurons by cyclin-dependent kinase CDK5 at Ser-270 is dependent on collybistin. *The Journal of biological chemistry* 287(37):30952-30966.
38. Kalbounieh H, Schlicksupp A, Kirsch J, & Kuhse J (2014) Cyclin-dependent kinase 5 is involved in the phosphorylation of gephyrin and clustering of GABAA receptors at inhibitory synapses of hippocampal neurons. *PloS one* 9(8):e104256.
39. Costa JT, *et al.* (2015) Gephyrin Cleavage in In Vitro Brain Ischemia Decreases GABA Receptor Clustering and Contributes to Neuronal Death. *Molecular neurobiology*.
40. Kumar A, *et al.* (2017) S-sulfocysteine/NMDA receptor-dependent signaling underlies neurodegeneration in molybdenum cofactor deficiency. *The Journal of clinical investigation*.
41. Yoong YL, Lee HS, Gwee MC, & Wong PT (1986) Acute tolerance to diazepam in mice: pharmacokinetic considerations. *Clinical and experimental pharmacology & physiology* 13(2):153-158.
42. Van Sickle BJ, Xiang K, & Tietz EI (2004) Transient plasticity of hippocampal CA1 neuron glutamate receptors contributes to benzodiazepine withdrawal-anxiety. *Neuropsychopharmacology : official publication of the American College of Neuropsychopharmacology* 29(11):1994-2006.
43. Xie XH & Tietz EI (1992) Reduction in potency of selective gamma-aminobutyric acidA agonists and diazepam in CA1 region of in vitro hippocampal slices from chronic flurazepam-treated rats. *The Journal of pharmacology and experimental therapeutics* 262(1):204-211.
44. Markowitz GJ, Kadam SD, Boothe DM, Irving ND, & Comi AM (2010) The pharmacokinetics of commonly used antiepileptic drugs in immature CD1 mice. *Neuroreport* 21(6):452-456.
45. Lorenz-Guertin JM, *et al.* (2017) A versatile optical tool for studying synaptic GABAA receptor trafficking. *J Cell Sci*.
46. Szent-Gyorgyi C, *et al.* (2008) Fluorogen-activating single-chain antibodies for imaging cell surface proteins. *Nature biotechnology* 26(2):235-240.
47. Szent-Gyorgyi C, *et al.* (2013) Malachite green mediates homodimerization of antibody VL domains to form a fluorescent ternary complex with singular symmetric interfaces. *Journal of molecular biology* 425(22):4595-4613.
48. Pratt CP, *et al.* (2017) Tagging of Endogenous BK Channels with a Fluorogen-Activating Peptide Reveals beta4-Mediated Control of Channel Clustering in Cerebellum. *Frontiers in cellular neuroscience* 11:337.
49. Wafford KA, *et al.* (1996) Functional characterization of human gamma-aminobutyric acidA receptors containing the alpha 4 subunit. *Molecular pharmacology* 50(3):670-678.
50. Tretter V, *et al.* (2008) The clustering of GABA(A) receptor subtypes at inhibitory synapses is facilitated via the direct binding of receptor alpha 2 subunits to gephyrin. *J Neurosci* 28(6):1356-1365.
51. Förster T (1965) Delocalized excitation and excitation transfer (Academic Press Inc., New York).
52. Gunther U, *et al.* (1995) Benzodiazepine-insensitive mice generated by targeted disruption of the gamma 2 subunit gene of gamma-aminobutyric acid type A receptors. *Proceedings of the National Academy of Sciences of the United States of America* 92(17):7749-7753.
53. Chaumont S, *et al.* (2013) Agonist-dependent endocytosis of gamma-aminobutyric acid type A (GABAA) receptors revealed by a gamma2(R43Q) epilepsy mutation. *The Journal of biological chemistry* 288(39):28254-28265.
54. Nicholson MW, *et al.* (2018) Diazepam-induced loss of inhibitory synapses mediated by PLCδ/Ca2+/calceineurin signalling downstream of GABAA receptors. *Molecular psychiatry*.

55. Brady ML, *et al.* (2017) Depolarizing, inhibitory GABA type A receptor activity regulates GABAergic synapse plasticity via ERK and BDNF signaling. *Neuropharmacology* 128:324-339.
56. Kawasaki BT, Hoffman KB, Yamamoto RS, & Bahr BA (1997) Variants of the receptor/channel clustering molecule gephyrin in brain: distinct distribution patterns, developmental profiles, and proteolytic cleavage by calpain. *Journal of neuroscience research* 49(3):381-388.
57. Vlachos A, Reddy-Alla S, Papadopoulos T, Deller T, & Betz H (2013) Homeostatic regulation of gephyrin scaffolds and synaptic strength at mature hippocampal GABAergic postsynapses. *Cerebral cortex* 23(11):2700-2711.
58. Renner M, Schweizer C, Bannai H, Triller A, & Levi S (2012) Diffusion barriers constrain receptors at synapses. *PloS one* 7(8):e43032.
59. Niwa F, *et al.* (2012) Gephyrin-independent GABA(A)R mobility and clustering during plasticity. *PloS one* 7(4):e36148.
60. Gonzalez MI, Cruz Del Angel Y, & Brooks-Kayal A (2013) Down-regulation of gephyrin and GABAA receptor subunits during epileptogenesis in the CA1 region of hippocampus. *Epilepsia* 54(4):616-624.
61. Bannai H, *et al.* (2015) Bidirectional Control of Synaptic GABAAR Clustering by Glutamate and Calcium. *Cell reports* 13(12):2768-2780.
62. Mukherjee J, *et al.* (2011) The residence time of GABA(A)Rs at inhibitory synapses is determined by direct binding of the receptor alpha1 subunit to gephyrin. *The Journal of neuroscience : the official journal of the Society for Neuroscience* 31(41):14677-14687.
63. Mukherjee J, *et al.* (2017) Estradiol modulates the efficacy of synaptic inhibition by decreasing the dwell time of GABAA receptors at inhibitory synapses. *Proceedings of the National Academy of Sciences of the United States of America* 114(44):11763-11768.
64. Levi S, Le Roux N, Eugene E, & Poncer JC (2015) Benzodiazepine ligands rapidly influence GABAA receptor diffusion and clustering at hippocampal inhibitory synapses. *Neuropharmacology* 88:199-208.
65. Gouzer G, Specht CG, Allain L, Shinoe T, & Triller A (2014) Benzodiazepine-dependent stabilization of GABA(A) receptors at synapses. *Mol Cell Neurosci* 63:101-113.
66. Nakamura Y, *et al.* (2016) Proteomic characterization of inhibitory synapses using a novel pHluorin-tagged GABAAR alpha2 subunit knock-in mouse. *The Journal of biological chemistry*.
67. Ge Y, *et al.* (2018) Clptm1 Limits Forward Trafficking of GABAA Receptors to Scale Inhibitory Synaptic Strength. *Neuron* 97(3):596-610.e598.
68. Uezu A, *et al.* (2016) Identification of an elaborate complex mediating postsynaptic inhibition. *Science (New York, N.Y.)* 353(6304):1123-1129.
69. Kang Y, *et al.* (2014) A combined transgenic proteomic analysis and regulated trafficking of neuroligin-2. *The Journal of biological chemistry* 289(42):29350-29364.
70. Butko MT, *et al.* (2013) In vivo quantitative proteomics of somatosensory cortical synapses shows which protein levels are modulated by sensory deprivation. *Proceedings of the National Academy of Sciences of the United States of America* 110(8):E726-735.
71. Churn SB, *et al.* (2002) Calcium/calmodulin-dependent kinase II phosphorylation of the GABAA receptor alpha1 subunit modulates benzodiazepine binding. *Journal of neurochemistry* 82(5):1065-1076.
72. Saliba RS, Kretschmannova K, & Moss SJ (2012) Activity-dependent phosphorylation of GABAA receptors regulates receptor insertion and tonic current. *Embo j* 31(13):2937-2951.
73. Marsden KC, Shemesh A, Bayer KU, & Carroll RC (2010) Selective translocation of Ca²⁺/calmodulin protein kinase IIalpha (CaMKIIalpha) to inhibitory synapses. *Proceedings of the National Academy of Sciences of the United States of America* 107(47):20559-20564.
74. Nakamura T, *et al.* (2016) PX-RICS-deficient mice mimic autism spectrum disorder in Jacobsen syndrome through impaired GABAA receptor trafficking. *Nat Commun* 7:10861.

75. Qian Z, Micorescu M, Yakhnitsa V, & Barmack NH (2012) Climbing fiber activity reduces 14-3-3-theta regulated GABA(A) receptor phosphorylation in cerebellar Purkinje cells. *Neuroscience* 201:34-45.
76. van Rijnsoever C, *et al.* (2004) Requirement of alpha5-GABAA receptors for the development of tolerance to the sedative action of diazepam in mice. *The Journal of neuroscience : the official journal of the Society for Neuroscience* 24(30):6785-6790.
77. Bachhuber MA, Hennessy S, Cunningham CO, & Starrels JL (2016) Increasing Benzodiazepine Prescriptions and Overdose Mortality in the United States, 1996-2013. *American journal of public health* 106(4):686-688.

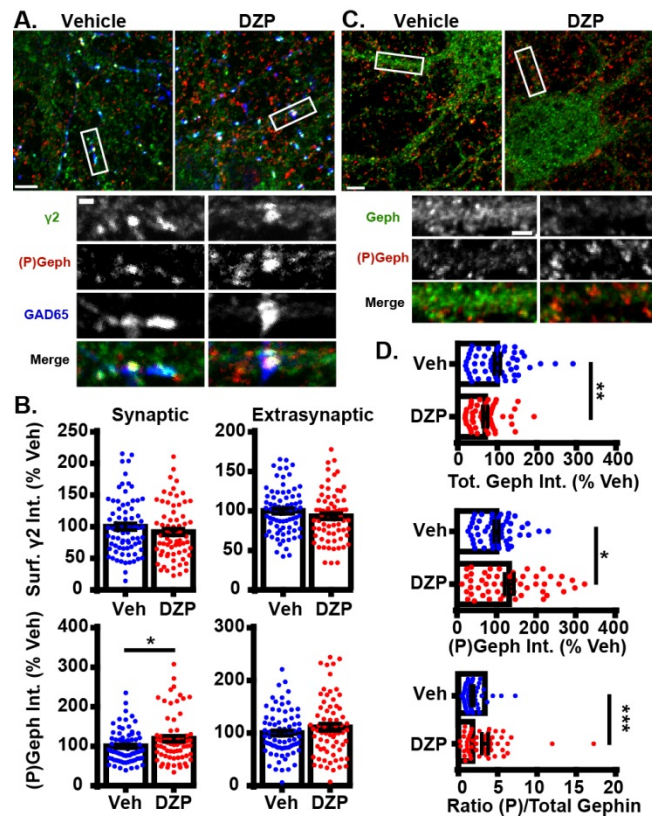


Figure 1. DZP downregulates gephyrin independent of $\gamma 2$ surface levels. A. Cortical neurons were treated for 24 h with vehicle or 1 μ M DZP, then immunostained for surface $\gamma 2$ GABA_AR (green), followed by permeabilization and immunostaining for (P)S270 gephyrin (red), and GAD65 (blue). Panels below show enlargements of GABA_AR synapses. B. Surface synaptic and extrasynaptic $\gamma 2$ levels are not significantly altered by DZP. Synaptic phospho-gephyrin was enhanced in response to DZP (n=69-74 neurons; 4 independent cultures). C. Neurons were treated as in A followed by antibody staining for total gephyrin (green) and (P)S270 gephyrin (red). Panels below show enlargements of dendrite region. D. The dendritic pool of gephyrin was decreased, while (P)S270 gephyrin levels were augmented, resulting in a dramatic increase in the ratio of phosphorylated gephyrin to total gephyrin (n=52-59 neurons; 3 independent cultures). Image scale bars: main panels = 5 μ m, enlargements = 1 μ m. * $p \leq 0.05$, ** $p < 0.01$, *** $p < 0.00$, Student's t-test; error bars \pm s.e.m.

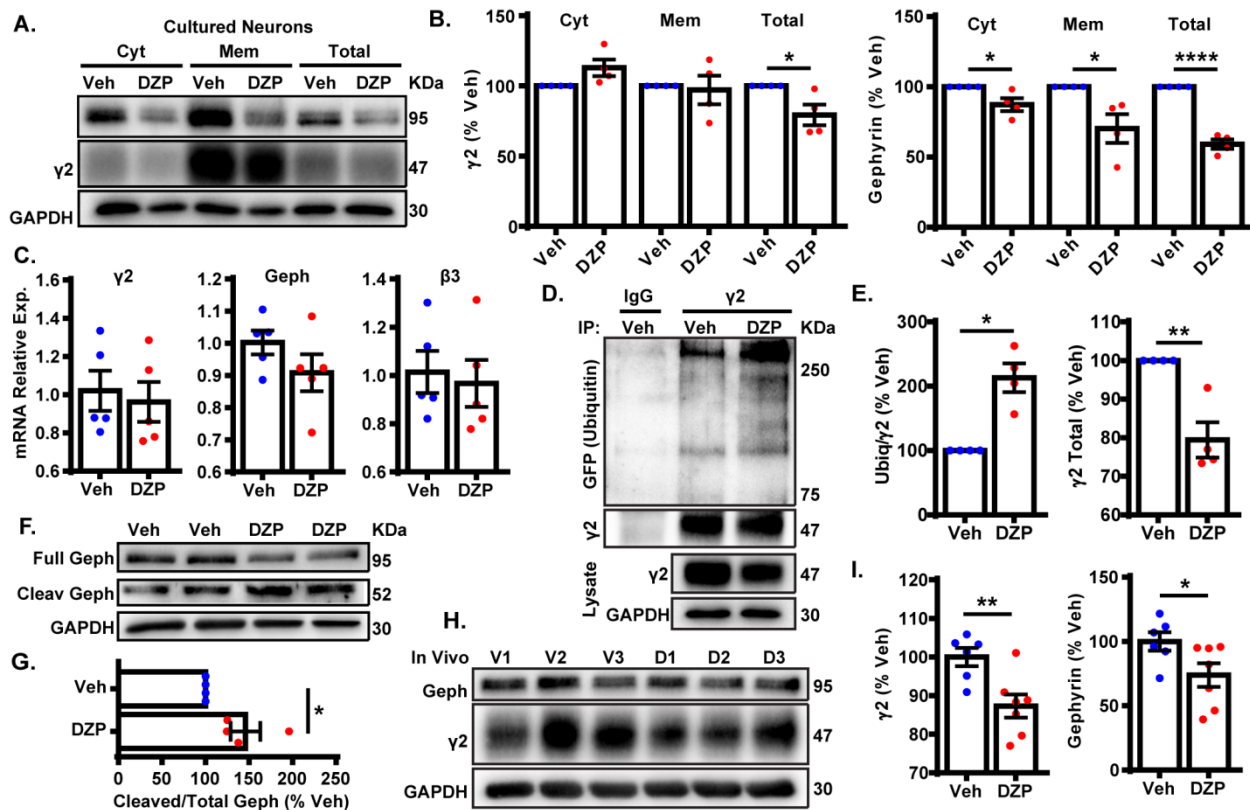


Figure 2. DZP induces degradation of $\gamma 2$ and gephyrin in vitro and in vivo. A. Cortical neurons exposed to 1 μ M DZP or vehicle for 24 h were subjected to membrane fraction and western blot analysis. B. Total $\gamma 2$ subunit and cytosolic, membrane, and total gephyrin were significantly reduced after DZP (n=4 independent cultures). C. Quantitative RT-PCR revealed no change in $\gamma 2$ subunit, $\beta 3$ subunit or gephyrin mRNA expression following 24 h DZP in vitro (n=5 independent cultures). D. GFP-ubiquitin transfected neurons were treated with vehicle or DZP for 12 h. Lysates were immunoprecipitated with control IgG or $\gamma 2$ antibody, followed by blotting with anti-GFP, $\gamma 2$ and GAPDH. E. DZP treatment increased the levels of $\gamma 2$ ubiquitin conjugates and decreased $\gamma 2$ total levels. F,G. DZP treatment enhanced the ratio of cleaved gephyrin fragments/full length gephyrin (n=4 independent cultures). H. Western blots of cortical tissue collected from mice 12 h after a single IP injection of 10 mg/kg DZP or vehicle. I. $\gamma 2$ subunit and gephyrin totals are significantly reduced in DZP-treated animals (6-7 mice per condition). (*p \leq 0.05, **p < 0.01, ****p < 0.0001, Student's t-test; error bars \pm s.e.m)

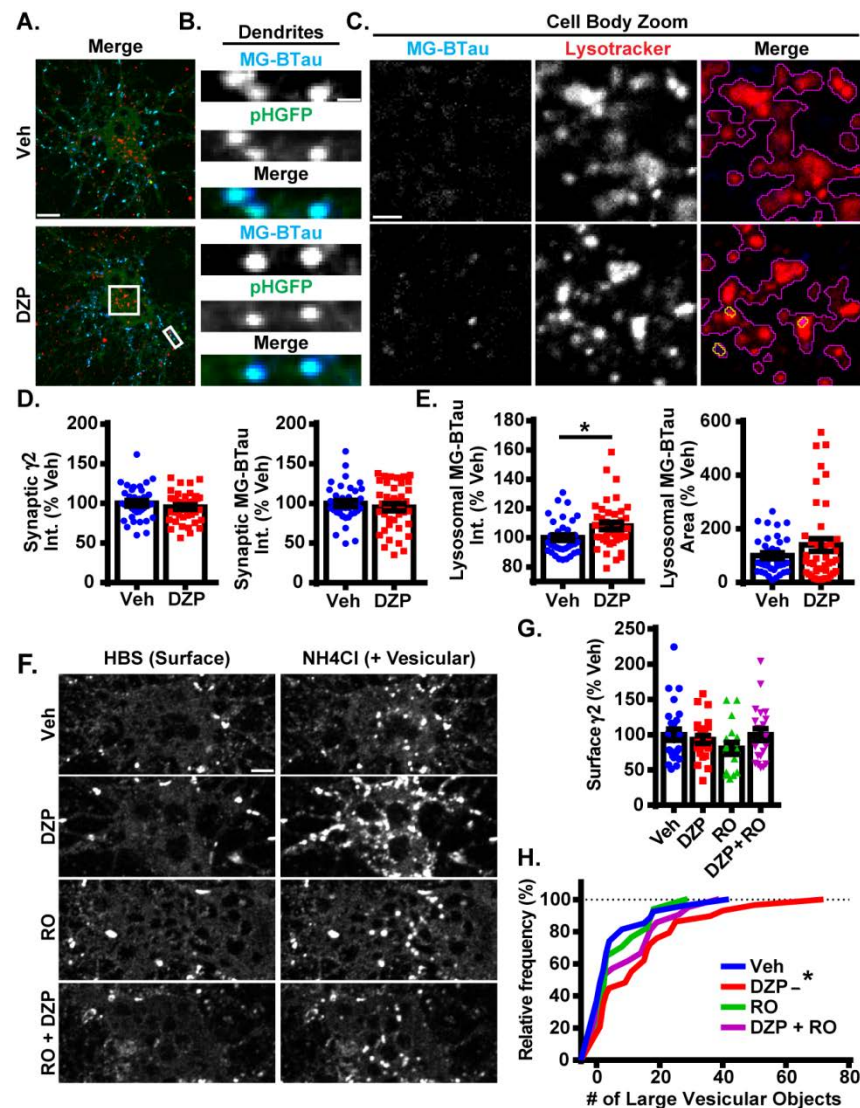


Figure 3. Lysosomal targeting and vesicular accumulation of $\gamma 2$ -GABA_ARs in response to DZP. A. $\gamma 2^{\text{pH}}$ FAP neurons were pretreated for 12-18 h with 1 μM DZP, then pulse-labeled with 100 nM MG-BTau dye for 2 min, and returned to conditioned media at 37°C +/- DZP for 1 h. 50 nM Lysotracker dye was added at the 30 min mark to identify lysosomes. MG-BTau = blue; pHGFP = green; Lysotracker = red. (n=37-42 neurons; 5 independent cultures). B. Dendrite zoom images show MG-BTau labeling at $\gamma 2^{\text{pH}}$ FAP synapses. C. Cell body zoom images highlighting colocalization of MG-BTau labeled GABA_ARs (yellow trace) at lysosomes (purple trace). D. pHGFP and MG-BTau measurements reveal surface synaptic $\gamma 2$ -GABA_AR levels are not altered by DZP. E. The pool of internalized MG-BTau GABA_ARs colocalized at lysosomes was enhanced in DZP treated neurons as measured by intensity (* $p \leq 0.05$, Student's t-test; error bars \pm s.e.m). F. Neurons treated 20-28 h with vehicle or DZP. The DZP site antagonist Ro 15-1788 (5 μM) was added 1-2 h prior to imaging to inhibit DZP binding at GABA_ARs. Neurons were first imaged in HBS, and then perfused with NH₄Cl (pH 7.4) to reveal intracellular $\gamma 2^{\text{pH}}$ FAP receptors. DZP treated neurons accumulated more $\gamma 2$ -GABA_ARs in large vesicular structures

compared to vehicle. (n=20-27 neurons; 3-4 independent cultures). G. Surface intensity of $\gamma 2^{\text{pH}}$ FAP was not different between treatments (one-way ANOVA; error bars \pm s.e.m). H. DZP-treated neurons more frequently demonstrated accumulation of $\gamma 2^{\text{pH}}$ FAP in large vesicles (*p \leq 0.05 Kolmogorov-Smirnov statistical test). Scale bars in μm : A=10; B=1; C=2, F=5.

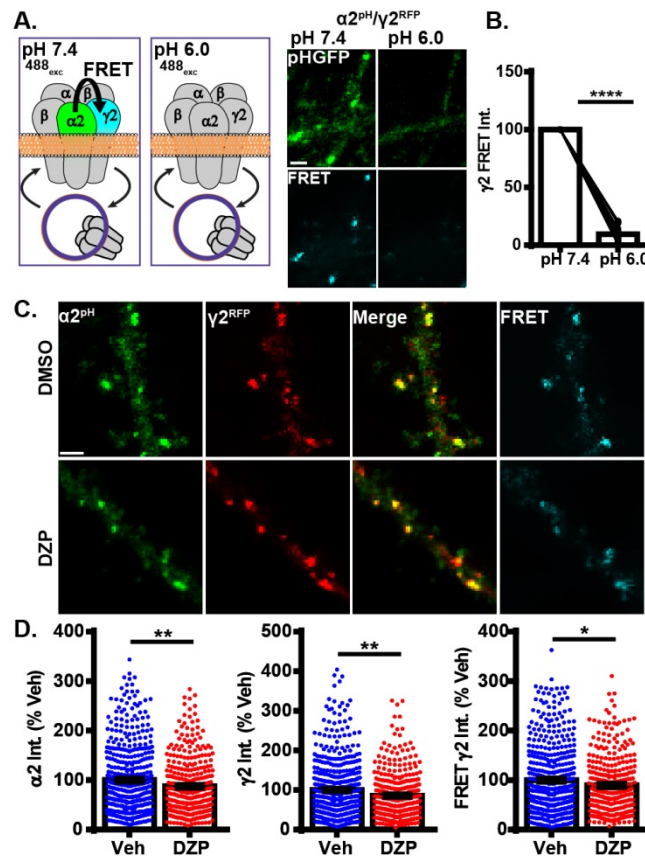


Figure 4. Intermolecular FRET reveals decreased synaptic $\alpha 2/\gamma 2$ surface GABA_ARs after DZP. A. Diagram and time-series images of cortical neurons expressing donor $\alpha 2^{pH}$ (green) and acceptor $\gamma 2^{RFP}$ during imaging and with imaging saline at pH 7.4 and pH 6.0. Surface $\alpha 2^{pH}$ (green) signal and intermolecular FRET (teal) between $\alpha 2/\gamma 2$ subunits occurs at pH 7.4, but is eliminated by brief wash with pH 6.0 extracellular saline and quenching of the $\alpha 2^{pH}$ donor pHGFP fluorescence. B. Quantification of relative FRET at pH 7.4 and pH 6.0 ($n = 20$ synapses). C. Neurons $\alpha 2^{pH}$ (green) and $\gamma 2^{RFP}$ (red) were treated with vehicle or DZP for 20-28 h +/- and then subjected to live-imaging. For each cell, an initial image used 488 nm laser excitation to identify surface $\alpha 2^{pH}$ and FRET $\gamma 2^{RFP}$. A second image was taken immediately afterwards to acquire $\gamma 2^{RFP}$ total levels (561 nm laser excitation). Dendritic lengths show multiple synaptic clusters with $\alpha 2/\gamma 2$ surface GABA_ARs. D. Synaptic cluster intensity quantification of $\alpha 2^{pH}$, $\gamma 2^{RFP}$ and FRET $\gamma 2^{RFP}$ (at least 15 synapses per cell; $n = 335-483$ synapses; 6 independent cultures). Image scale bars = 2 μm (* $p \leq 0.05$, ** $p < 0.01$, **** $p < 0.0001$, paired t-test (B), Student's t-test (D); error bars \pm s.e.m.).

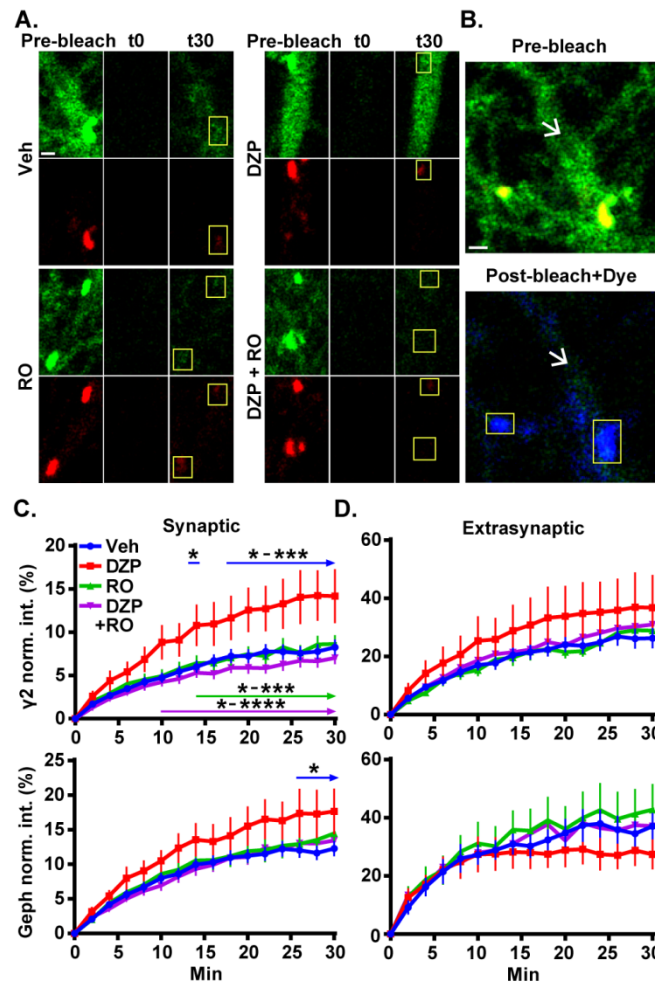


Figure 5. Prolonged DZP exposure accelerates $\gamma 2$ GABA_A R and gephyrin synaptic exchange. A. Neurons expressing $\gamma 2^{\text{pH}}$ FAP GABA_A R (green) and RFP-gephyrin (red) were treated with vehicle or DZP for 20-28 h +/- Ro 15-1788 for the last 1-2 h. Neurons were imaged at 37°C in constant presence of treatment. Initial image taken prior to photobleaching (Pre-bleach), then imaged post-bleach (t0) every 2 min for 30 min. Images of dendritic regions show synaptic cluster sites (yellow boxes) and extrasynaptic regions. B. 10 nM MG-BTau dye (blue) was added immediately after bleaching events in A. to resolve bleached $\gamma 2^{\text{pH}}$ FAP GABA_A Rs and provide spatial accuracy for time series measurements. Yellow box indicates synaptic cluster site, and arrows indicates extrasynaptic region. C, D. Fluorescence recovery of $\gamma 2$ GABA_A R and gephyrin measured at synaptic sites and extrasynaptic sites from A. Synapse = $\gamma 2^{\text{pH}}$ FAP cluster colocalized with gephyrin cluster. Image scale bars = 1 μm (* $p \leq 0.05$, ** $p < 0.01$, *** $p < 0.001$, **** $p < 0.0001$, two-way ANOVA; Tukey's multiple comparisons test; 4-8 synapses and one 10 μm extrasynaptic region per cell; 51-56 synapses from 16 neurons per treatment; 4 independent cultures; error bars \pm s.e.m).

Table 1. Proteins Demonstrating Increased Association with γ 2-GABA_ARs after DZP In Vivo by Mass Spectrometry.

<i>Ratio DZP/V</i>	<i>P-Value</i>	<i>UniProtKB</i>	<i>Gene ID</i>	<i>Entrez Gene Name</i>	<i>Location</i>	<i>Type(s)</i>
9.6	8.9E-02	Q14BI2	GRM2	glutamate metabotropic receptor 2	Plasma Membrane	G-protein coupled receptor
9.5	4.3E-02	P12960	CNTN1	contactin 1	Plasma Membrane	enzyme
7.0	5.9E-02	P11276	FN1	fibronectin 1	Extracellular Space	enzyme
5.4	2.7E-02	E9Q4P0	KXD1	KxDL motif containing 1	Cytoplasm	other
5.4	3.1E-02	Q62277	SYP	synaptophysin	Cytoplasm	transporter
5.0	5.0E-03	Q9QXY6	EHD3	EH domain containing 3	Cytoplasm	other
5.0	7.8E-02	P48774	GSTM3	glutathione S-transferase mu 3	Cytoplasm	enzyme
4.9	1.9E-05	P38647	HSPA9	heat shock protein family A (Hsp70) member 9	Cytoplasm	other
4.7	6.4E-02	Q91V41	RAB14	RAB14, member RAS oncogene family	Cytoplasm	enzyme
4.2	6.4E-02	P48758	CBR1	carbonyl reductase 1	Cytoplasm	enzyme
4.2	7.2E-02	Q8K3F6	KCNQ3	potassium voltage-gated channel subfamily Q member 3	Plasma Membrane	ion channel
4.2	3.3E-02	A0A0R4J036	Nefm	neurofilament, medium polypeptide	Plasma Membrane	other
4.0	7.9E-02	Q92111	TF	transferrin	Extracellular Space	transporter
3.8	8.6E-02	Q9CYZ2	TPD52L2	tumor protein D52 like 2	Cytoplasm	other
3.3	4.2E-02	Q99KI0	ACO2	aconitase 2	Cytoplasm	enzyme
2.6	8.0E-02	Q9EQF6	DPYSL5	dihydropyrimidinase like 5	Cytoplasm	enzyme
2.4	2.2E-02	P56480	ATP5F1B	ATP synthase F1 subunit beta	Cytoplasm	transporter
2.4	9.2E-02	P46096	SYT1	synaptotagmin 1	Cytoplasm	transporter
2.4	3.7E-02	Q6P1J1	CRMP1	collapsin response mediator protein 1	Cytoplasm	enzyme
2.2	3.8E-02	Q9DB20	ATP5PO	ATP synthase peripheral stalk subunit OSCP	Cytoplasm	transporter
1.9	N.A.	P61027	RAB10	RAB10, member RAS oncogene family	Cytoplasm	enzyme
1.8	9.6E-02	P63017	HSPA8	heat shock protein family A (Hsp70) member 8	Cytoplasm	enzyme
1.8	1.8E-02	P63011	RAB3A	RAB3A, member RAS oncogene family	Cytoplasm	enzyme
1.8	1.3E-02	P17426-2	AP2A1	adaptor related protein complex 2 subunit alpha 1	Cytoplasm	transporter
1.7	9.1E-02	P18760	CFL1	cofilin 1	Nucleus	other
1.7	8.2E-02	Q9Z219	SUCLA2	succinate-CoA ligase ADP-forming beta subunit	Cytoplasm	enzyme
1.7	4.0E-02	P63328	PPP3CA	protein phosphatase 3 catalytic subunit alpha	Cytoplasm	phosphatase
1.7	7.1E-02	Q8R191	SYNGR3	synaptogyrin 3	Plasma Membrane	other
1.6	5.7E-02	Q8BHJ7	GABRA5	gamma-aminobutyric acid type A receptor alpha5 subunit	Plasma Membrane	ion channel
1.6	1.8E-02	O35129	PHB2	prohibitin 2	Cytoplasm	transcription regulator
1.6	1.6E-02	P61982	YWHAG	tyrosine 3-monooxygenase/tryptophan 5-monooxygenase activation protein gamma	Cytoplasm	other
1.5	5.3E-02	P07901	HSP90A A1	heat shock protein 90 alpha family class A member 1	Cytoplasm	enzyme
1.5	7.8E-03	P67778	PHB	prohibitin	Nucleus	transcription regulator
1.5	8.1E-02	Q3UGC7	EIF3J	eukaryotic translation initiation factor 3 subunit J	Cytoplasm	translation regulator
1.5	7.5E-02	Q8VEM8	SLC25A3	solute carrier family 25 member 3	Cytoplasm	transporter

1.3	3.3E-02	P60710	ACTB	actin beta	Cytoplasm	other
NF-V	7.9E-04	P62259	YWHAE	tyrosine 3-monooxygenase/tryptophan 5-monooxygenase activation protein epsilon	Cytoplasm	other
NF-V	1.0E-02	P63044	VAMP2	vesicle associated membrane protein 2	Plasma Membrane	other
NF-V	1.6E-02	P46660	INA	internexin neuronal intermediate filament protein alpha	Cytoplasm	other
NF-V	3.7E-02	Q9QYM9	TMEFF2	transmembrane protein with EGF like and two follistatin like domains 2	Cytoplasm	other
NF-V	4.1E-02	Q6PHN9	RAB35	RAB35, member RAS oncogene family	Cytoplasm	enzyme
NF-V	6.0E-02	P19246	NEFH	neurofilament heavy	Cytoplasm	other
NF-V	6.3E-02	Q9CZ13	UQCRC1	ubiquinol-cytochrome c reductase core protein 1	Cytoplasm	enzyme
NF-V	1.2E-06	Q9CQQ7	ATP5PB	ATP synthase peripheral stalk-membrane subunit b	Cytoplasm	transporter
NF-V	2.8E-06	P80317	CCT6A	chaperonin containing TCP1 subunit 6A	Cytoplasm	other
NF-V	2.8E-06	Q9CWS0	DDAH1	dimethylarginine dimethylaminohydrolase 1	Cytoplasm	enzyme

Ratio DZP/V is fold change in DZP animals' peptide spectral counts (SC) relative to control vehicle treated animals. NF-V = not found in vehicle samples. n=3 animals per treatment condition, P<0.1, t-test.

Table 2. Proteins Demonstrating Decreased Association with γ 2-GABA_ARs after DZP In Vivo by Mass Spectrometry.

<i>Ratio DZP/V</i>	<i>P-Value</i>	<i>UniProtKB</i>	<i>Gene ID</i>	<i>Entrez Gene Name</i>	<i>Location</i>	<i>Type(s)</i>
0.2	3.4E-02	P62717	RPL18A	ribosomal protein L18a	Cytoplasm	other
0.2	3.9E-02	P62874	GNB1	G protein subunit beta 1	Plasma Membrane	enzyme
0.2	4.2E-02	Q60900-2	ELAVL3	ELAV like RNA binding protein 3	Nucleus	other
0.2	5.8E-02	Q920I9	WDR7	WD repeat domain 7	Cytoplasm	other
0.3	2.0E-02	P53026	RPL10A	ribosomal protein L10a	Nucleus	other
0.3	3.4E-02	Q91VM5	Rbmxl1	RNA binding motif protein, X-linked like-1	Nucleus	other
0.4	6.9E-02	P49312	Hnrnpa1	heterogeneous nuclear ribonucleoprotein A1	Nucleus	other
0.4	8.5E-02	Q8BG05	Hnrnpa3	heterogeneous nuclear ribonucleoprotein A3	Nucleus	transporter
0.4	7.9E-02	Q922F4	TUBB6	tubulin beta 6 class V	Cytoplasm	other
0.5	5.2E-02	P62334	PSMC6	proteasome 26S subunit, ATPase 6	Nucleus	peptidase
0.5	2.9E-04	P11798	CAMK2A	calcium/calmodulin dependent protein kinase II alpha	Cytoplasm	kinase
0.5	3.6E-02	E9PV14	EPB41L1	erythrocyte membrane protein band 4.1 like 1	Plasma Membrane	other
0.7	6.8E-02	P16330	CNP	2',3'-cyclic nucleotide 3' phosphodiesterase	Cytoplasm	enzyme
0.7	7.6E-02	O35643	AP1B1	adaptor related protein complex 1 subunit beta 1	Cytoplasm	transporter
0.8	1.4E-02	P68369	TUBA1A	tubulin alpha 1a	Cytoplasm	other
0.8	8.0E-02	P52480	PKM	pyruvate kinase M1/2	Cytoplasm	kinase
NF-DZP	1.5E-02	P61358	RPL27	ribosomal protein L27	Cytoplasm	other
NF-DZP	3.5E-02	Q9Z1X4-3	ILF3	interleukin enhancer binding factor 3	Nucleus	transcription regulator
NF-DZP	5.5E-02	Q80UJ0	ELAVL2	ELAV like RNA binding protein 2	Cytoplasm	other
NF-DZP	2.8E-06	Q3UHB8	CCDC177	coiled-coil domain containing 177	Other	other
NF-DZP	2.8E-06	P49615	CDK5	cyclin dependent kinase 5	Nucleus	kinase
NF-DZP	2.8E-06	Q6ZWV3	RPL10	ribosomal protein L10	Cytoplasm	translation regulator
NF-DZP	2.8E-06	Q9CQ69	UQCRQ	ubiquinol-cytochrome c reductase complex III subunit VII	Cytoplasm	enzyme

Ratio DZP/V is fold change in DZP animals' peptide SC relative to control vehicle treated animals. NF-DZP = not found in DZP samples. n=3 animals per treatment condition, P<0.1, t-test.

Figure 6. Ingenuity Pathway Analysis Reveals Shifts in Protein Interaction Networks Following DZP Exposure. (A) Canonical pathways found to be enriched with $\gamma 2$ -GABA_ARs and differentially expressed following DZP administration in vivo. Enriched pathways with $-\log(p\text{-value})$ greater than 6.2 were considered as calculated by Fisher's exact test right-tailed. Values to right of bars represent pathway activation z-score. Positive z-score represents predicted upregulation of a pathway (orange), negative z-score predicts inhibition (blue), z-score = 0 represents no change in pathway (white), while not determined (N.D.) conveys the analysis program was unable to determine a significant change (grey). Intensity of color represents size of z-score value. (B) Functional pathway network analysis revealed that DZP treatment resulted in increased $\gamma 2$ -GABA_AR association with proteins involved in endocytosis, developmental process of the synapse, cell-cell contact, and quantity of cell-cell contacts (activation z-score > 2.5). Red = increased measurement, green = decreased measurement, orange = activation of pathway, yellow = findings inconsistent with state of downstream molecule, grey = effect not predicated.

Table 3. GO Analysis Reveals Enrichment of Intracellular Trafficking, Transport, and Protein Localization Pathways after DZP.

<i>GO Biological Process</i>	<i>GO Term ID</i>	<i>Fold Enrichment</i>	<i>P-Value</i>
transport	GO:0006810	4.2	9.8E-09
establishment of localization	GO:0051234	4.0	2.5E-08
establishment of localization in cell	GO:0051649	6.8	2.0E-07
localization	GO:0051179	3.3	2.5E-07
intracellular transport	GO:0046907	7.2	1.6E-06
regulation of localization	GO:0032879	4.3	3.7E-06
intracellular protein transport	GO:0006886	9.1	7.8E-06
regulation of transport	GO:0051049	5.1	2.2E-05
cellular localization	GO:0051641	4.8	4.8E-05
protein transport	GO:0015031	6.1	2.2E-04

Proteins found to have enhanced association ($P < 0.1$) with $\gamma 2$ -GABA_ARs during Scaffold analysis were searched in the GO Ontology database for biological process pathway enrichments. PANTHER Overrepresentation test and Fisher's Exact test with Bonferroni correction for multiple testing was used to determine significance.

Supporting Information

Materials and Methods

Cell Culture, Transfection, Expression Constructs and Mice. Cortical neurons were prepared from embryonic day 18 rats, nucleofected with constructs at plating (Amaxa). The $\gamma 2^{\text{pH}}$ FAP construct was characterized in (1) and RFP-gephyrin was described in (2). The $\gamma 2^{\text{RFP}}$ construct was generated by PCR cloning and fully sequenced: the red fluorescent protein mCherry replaced pHluorin in the previously published $\gamma 2^{\text{pHGFP}}$ construct (2). GFP-ubiquitin was a gift from Nico Dantuma (Addgene plasmid # 11928) (3). 8-10 week old male C57BL/6J mice (Jackson Laboratory) were maintained on a reverse 12 h dark/light schedule. Mouse cortical brain tissue was collected and flash frozen 12 h after I.P. injection with either vehicle or diazepam (in 40% PEG, 10% EtOH, 5% Na Benzoate, 1.5 % benzyl alcohol (Hospira)). All procedures were approved by the University of Pittsburgh Institutional Animal Care and Use Committee.

Reagents, Antibodies, and MG Dye. Diazepam (cell culture, Sigma; injections, Hospira); Ro 15-1788 (Tocris Bioscience); calpain-1 inhibitor MDL-28170 (Santa Cruz); L-glutamic acid (Tocris Bioscience). Primary antibodies: GAPDH (14C10, Cell Signaling); GAD-65 (198104, Synaptic Systems); $\gamma 2$ GABA_AR subunit (224003, Synaptic Systems); gephyrin (sc-14003, Santa Cruz); gephyrin (147002, Synaptic Systems); gephyrin mAb7a (147011, Synaptic Systems); GFP (GFP-1020, Aves). MG-BTau dye prepared as in (1).

Fixed and Live-Imaging. Measurements were made on days in vitro (DIV) 15–19 cortical neurons. Live-imaging performed in Hepes-buffered saline (HBS), containing the following (in mM): 135 NaCl, 4.7 KCl, 10 Hepes, 11 glucose, 1.2 MgCl₂, and 2.5 CaCl₂ (adjusted to pH 7.4 with NaOH). Images were acquired using a Nikon A1 confocal microscope with a 60× oil objective (N.A., 1.49) at 3× zoom. Data were analyzed in NIS Elements software (Nikon, N.Y.). Measurements were taken from whole cell or averaged from three dendritic 10μm regions of interest (ROI) per cell. For fixed imaging, media was quickly removed and coverslips were washed twice with Dulbecco's Phosphate Buffered Saline (DPBS) and immediately fixed with 4% paraformaldehyde and then blocked in PBS containing 10% fetal bovine serum and 0.5% bovine serum albumin. Surface antibody staining was performed under non-permeabilized conditions overnight at 4°C. Intracellular staining was performed overnight at 4°C following 0.2% Triton-X permeabilization for 10 min in blocking solution. Synaptic sites were determined during analysis by binary thresholds and colocalization with GAD-65. Extrasynaptic intensity was measured by taking the total dendrite ROI sum intensity minus background and synaptic fluorescence intensity. Dendritic fluorescence was measured using binary thresholds. Total Experimental conditions were blinded. The ROUT test (Q=1%) or Grubbs' Test (alpha=0.05) was used to remove a single outlier from a data set.

Lysosomal Targeting Assay. Neuron surface and lysosomal-association assays utilized MG-BTau dye for surface receptor pulse-labeling. DIV 15-16 neurons were treated with vehicle or DZP for 8-12 h, then pulse labeled with 100nM MG-BTau for 2 min at room temperature in HBS. Neurons were then washed 5x times with HBS and returned to conditioned media +/- DZP for 1h. To identify lysosomal targeting, 50 nM LysoTracker Blue DND-22 (Life Technologies)

and the lysosomal inhibitor, Leupeptin (200 μ M Amresco), was added 30 min prior to imaging. Following incubation, neurons were washed and imaged in 4°C HBS. Two-three neurons were immediately imaged per culture dish within 10 min of washing. For image analysis, independent ROIs were drawn to capture the soma, three 10 μ m sections of dendrite and the whole cell. Binary thresholds and colocalization measurements were performed to identify MG-BTau, pHGFP synaptic GABA_AR clusters and lysosomes. Total surface pHGFP expression was determined by taking the entire cell surface signal following background subtraction.

NH₄Cl Intracellular Imaging. DIV 15-16 neurons were washed and continuously perfused with HBS + treatment at room temperature. Multiposition acquisition was used to image 2-3 neurons per dish. An initial image was taken to identify surface $\gamma 2^{\text{pH}}$ FAP GABA_ARs. Neurons were then perfused with NH₄Cl solution to collapse the cellular pH gradient and were reimaged. NH₄Cl solution (in mM): 50 NH₄Cl, 85 NaCl, 4.7 KCl, 10 Hepes, 11 glucose, 1.2 MgCl₂, and 2.5 CaCl₂ (adjusted to pH 7.4 with NaOH). pHGFP intensity was measured following background subtraction and smoothing. Surface/total levels were determined by dividing the first image (surface only) from the second image (total). The spot detection tool in Nikon Elements was used to selectively count larger intracellular vesicles positive for $\gamma 2^{\text{pH}}$ FAP. A stringent threshold was set to identify brightly fluorescent circular objects with a circumference of approximately 0.75 μ m. Values reflect new vesicle objects that were only seen after NH₄Cl perfusion (second image – first image).

Intermolecular FRET Imaging, Characterization and Analysis. The $\alpha 2^{\text{pH}}$ pHGFP ($\alpha 2^{\text{pH}}$) construct was previously published (50) and the $\gamma 2^{\text{RFP}}$ construct was generated by PCR cloning and fully sequenced. DIV 15-16 neurons were treated with Veh or DZP for 20-28 h, then washed and continuously perfused with HBS at room temperature. Images were acquired with a 60x objective at 2x zoom. For each cell, an initial image was acquired containing two channels to identify surface $\alpha 2^{\text{pH}}$ (excited by 488 laser, emission band pass filter 500-550) and $\gamma 2^{\text{RFP}}$ participating in FRET (excited 488 FRET, emission band pass filter 575–625 nm, FRET channel). A second, single channel image was taken immediately following with only 561 nm excitation to reveal total $\gamma 2^{\text{RFP}}$ levels (excited by 561 laser, emission band pass filter 575–625 nm). For synaptic quantifications, binary thresholding based on intensity was applied with smoothing and size exclusion (0-3 μ m) factors. FRET and 561 channel binaries shared identical minimum and maximum binary threshold ranges. Individual synaptic ROIs were created to precisely target and measure synaptic clusters containing both $\alpha 2^{\text{pH}}$ and $\gamma 2^{\text{RFP}}$. Manual trimming and single pixel removal were used to remove signal not meeting the criteria of a receptor cluster. Restriction criteria were applied in the following order: 1) at least 15 synapses measured per cell, 2) FRET $\gamma 2^{\text{RFP}}$: raw $\gamma 2^{\text{RFP}}$ sum intensity ratio must be less than one, 3) synaptic $\alpha 2^{\text{pH}}$ mean intensity of at least 500, and 4) $\alpha 2^{\text{pH}}$ sum intensity limit of 300% of average sum intensity. ROI data was then normalized to vehicle control as percent change. The percentage of RFP participating in FRET was also calculated using FRET RFP:Total RFP ratio.

FRET activity was directly assessed by acceptor ($\gamma 2^{\text{RFP}}$) photobleaching. Photobleaching ROIs were implemented on 2 synapses per cell. Pre-bleaching images were acquired every 5 seconds, followed by a $\gamma 2^{\text{RFP}}$ photobleaching event using 80% 561 nm laser power. After photobleaching, image capturing resumed without delay using pre-bleach laser power settings for 2 minutes. Image analysis incorporated background subtraction and the measurement of percent change in $\alpha 2^{\text{pH}}$ /FRET $\gamma 2^{\text{RFP}}$ ratio over the time course. FRET efficacy measurements compared

directly adjacent $\alpha 2^{\text{pH}}$ and $\gamma 2^{\text{RFP}}$ subunits in a GABA_AR complex. Live-imaging with perfusion of pH 6.0 extracellular imaging saline solution (MES) was used to quench the pH-dependent GFP fluorescence from the $\alpha 2^{\text{pH}}$ donor fluorophores and show the dependence of FRET on surface $\alpha 2^{\text{pH}}$ fluorescence. Acidic extracellular saline solution, MES solution pH 6.0 (in mM): 10 MES, 135 NaCl, 4.7 KCl, 11 glucose, 1.2 MgCl₂, and 2.5 CaCl₂ (adjusted to pH 7.4 with NaOH). Images were collected under HBS conditions for 1 minute at 20 second intervals, and then followed by a 2 minute MES wash with the same imaging interval to quench donor emissions. FRET RFP mean intensity was measured under both conditions and normalized to HBS. Percent change in FRET RFP emissions were reported.

Synaptic Exchange Rate FRAP Imaging. Neurons were washed and media was replaced with HBS + treatment. Imaging was performed in an enclosed chamber at 37°C. An initial image was taken for baseline standardization. Photobleaching was performed by creating a stimulation ROI box encompassing two or more dendrites. This stimulation region was photobleached using the 488 and 561 lasers at 25% power for 1 minute. The same stimulation ROI was used for every cell in an experiment. Immediately following photobleaching, 10nM MG-Tau dye was added to the cell culture dish to reidentify surface synaptic GABA_AR clusters. Time-lapse imaging was then started every 2 min for 60 min. During image analysis, objects were only considered synaptic if they demonstrated colocalization with $\gamma 2^{\text{pH}}$ FAP pHGFP signal, RFP-gephyrin signal, and had obvious surface MG-BTau fluorescence. ROIs were drawn measuring the rate of fluorescence recovery at 4-8 synaptic sites and one extrasynaptic site (10 μ m long region; beizer tool) per cell. For data analysis, synapse post-bleach fluorescence intensity time point data was first normalized to pre-bleach fluorescence intensity (post-bleach/pre-bleach). Normalized synapse post-bleach data was then calculated as percent change from t₀ ((tx/t₀)*100, where x = min). Individual synapses were then averaged to calculate fluorescence recovery and statistically significant changes across time points.

Western Blot and Immunoprecipitation. Protein concentration was determined by BCA protein assay for all biochemistry. Neurons were lysed in denaturing buffer for immunoprecipitation: 50mM Tris HCl, 1mM EDTA, 1% SDS, 2mM Na₃VO₄, 10mM NaF, 50mM N-ethylmaleimide, protease inhibitor cocktail (Sigma). Lysates were sonicated and heated at 50°C for 20 min, then diluted 1:5 in RIPA buffer (50mM Tris HCl pH 7.6, 150mM NaCl, 1% Igepal, 0.5 % Sodium deoxycholate, 1mM EDTA, 2mM Na₃VO₄, 10mM NaF, 50mM N-ethylmaleimide, protease inhibitor cocktail). Standard immunoprecipitation procedures were performed using overnight incubation with $\gamma 2$ subunit antibody or rabbit IgG (sci2027; Sigma), 1 h incubation with protein A sepharose 4B beads (Invitrogen), three RIPA buffer washes, and loading for SDS-PAGE. After electrophoresis and transfer to nitrocellulose membrane, samples were probed with primary antibody overnight followed by the appropriate horseradish peroxidase (HRP)-coupled secondary antibody.

Membrane and Subcellular Fractionation. Cultured neurons were lysed using fractionation buffer: 50mM Tris-HCl, 50mM NaCl, 1mM EDTA, 2mM NaOV, 10mM NaF, 320mM sucrose, 0.25% igepal, and protease inhibitor cocktail. Lysates were spun at 50,000 RPM for 30 min at 4°C to separate pellet (plasma membrane) from supernatant (cytosol). Fraction integrity was tested by localization specific markers in all experiments (Supplementary Figure 1 and data not shown).

Coimmunoprecipitation. Mice were injected with vehicle control or 10mg/kg DZP and sacrificed 12 h post-injection (n=4 mice per treatment). Mouse cortical tissue was homogenized in coIP buffer (50mM Tris HCl pH 7.6, 50mM NaCl, 0.25% Igepal, 1mM EDTA, 2mM Na₃VO₄, 10mM NaF, 50mM N-ethylmaleimide, and Sigma protease inhibitor cocktail) using a Dounce homogenizer. Tissue was solubilized with end-over-end mixing at 4°C for 15 min, and then spun at 1,000g to remove non-solubilized fractions. Each immunoprecipitation tube contained 375µg of tissue lysate brought up to 1ml volume using coIP buffer. Lysates were precleared using Protein A-Sepharose 4B beads (Invitrogen) for 1 h at 4°C. Lysate was then immunoprecipitated overnight with 2.5µg rabbit γ2 subunit antibody (224003, Synaptic Systems) or 2.5µg rabbit IgG (2027, Santa Cruz). The next day, 40ul Protein A Sepharose slurry was added and mixed for 2 h at 4°C on a nutator. Beads were then washed 3x at 4°C on a nutator in 1ml coIP buffer. Beads were denatured with SDS-PAGE loading buffer [Laemmli Sample buffer (Biorad) + β-mercaptoethanol] with heat at 70°C for 10 min and intermittent vortexing. Two immunoprecipitation reactions were performed per animal and were pooled into a single tube without beads to be used for downstream in-gel digestion.

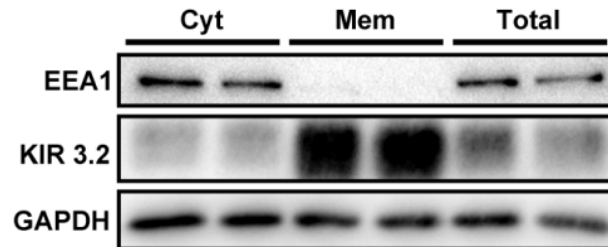
Mass Spectrometry and Data Processing. Immunoprecipitated proteins were separated by electrophoresis in Criterion XT MOPS 12% SDS-PAGE reducing gels (Bio-Rad), with subsequent protein visualization by staining with Coomassie blue. Each gel lane was divided into six slices. After de-staining, proteins in the gel slices were reduced with TCEP [tris(2-carboxyethyl)phosphine hydrochloride] and then alkylated with iodoacetamide before digestion with trypsin (Promega). HPLC-electrospray ionization-tandem mass spectrometry (HPLC-ESI-MS/MS) was accomplished by data-dependent acquisition on Thermo Fisher Orbitrap Fusion Lumos Tribrid mass spectrometer. Mascot (Matrix Science; London, UK) was used to search the MS files against the mouse subset of the UniProt database combined with a database of common contaminants. Subset searching of the Mascot data, determination of probabilities of peptide assignments and protein identifications, were accomplished by Scaffold (v 4.8.4, Proteome Software). MS data files for each entire gel lane were combined via the “MudPIT” option. Identification criteria were: minimum of two peptides; 96% peptide threshold; 1% FDR; 99% protein threshold. One vehicle- and one DZP-treated animal were removed from analysis due to insufficient γ2 subunit pulldown relative to all other groups. Protein clustering was applied in Scaffold and weighted spectrum values and exclusive unique peptides were exported for manual excel analysis. Student’s t-test analysis (P < 0.1) was performed using relative fold change (ratio) of DZP compared to vehicle group. In some cases peptides were only detected in vehicle or DZP treated groups, resulting in DZP/V ratio values of zero or undefined error (cannot divide by zero). These were annotated as NF-DZP (not found in DZP samples) or NF-V (not found in vehicle samples) in the tables.

Bioinformatics Analysis. Ingenuity Pathways Analysis (IPA) (Ingenuity Systems) was used for cellular pathway analysis. Relative fold levels of DZP proteins compared to vehicle were used for analysis. To be suitable for IPA analysis, proteins NF-DZP were assigned a value of -1E+99, while proteins NF-V were assigned a value of 1E+99. Significant enrichment in protein networks are calculated by right tailed Fisher's exact test. Z-score analysis is a statistical measure of an expected relationship direction and observed protein/gene expression to predict pathway activation or inhibition. IPA core analysis was searched to determine direct and indirect relationships within 35 molecules per network and 25 networks per analysis. All data repositories

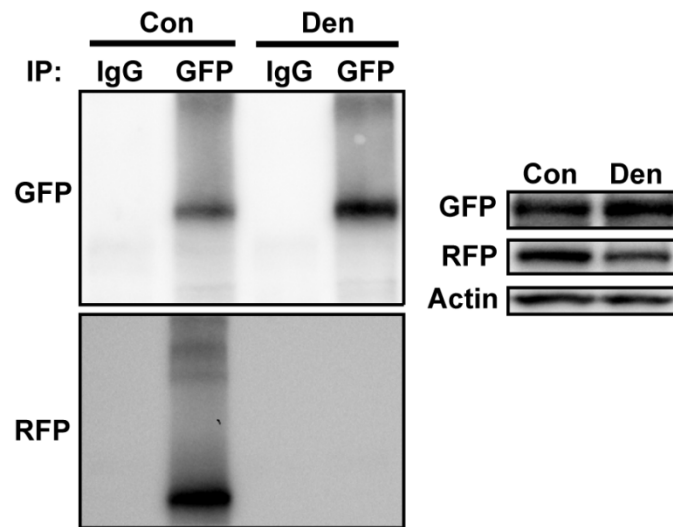
available through IPA were used to determine experimentally observed and highly predicted interactions occurring in mammalian tissue and cell lines. Ratio data were converted to fold change values in IPA, where the negative inverse ($-1/x$) was taken for values between 0 and 1, while ratio values greater than 1 were not affected. Proteins found to be significantly enhanced ($P < 0.1$) in their association with $\gamma 2$ were searched in the Mus musculus GO Ontology database (released 2018-10-08) for GO biological process and GO molecular function and analyzed by the PANTHER overrepresentation test; significance was determined using Fisher's Exact with Bonferroni correction for multiple testing.

1. Lorenz-Guertin JM, et al. (2017) A versatile optical tool for studying synaptic GABA_A receptor trafficking. *Journal of Cell Science* 130(22):3933-3945.
2. Brady ML & Jacob TC (2015) Synaptic localization of alpha5 GABA (A) receptors via gephyrin interaction regulates dendritic outgrowth and spine maturation. *Developmental neurobiology* 75(11):1241-1251.
3. Dantuma NP, Groothuis TA, Salomons FA, & Neefjes J (2006) A dynamic ubiquitin equilibrium couples proteasomal activity to chromatin remodeling. *The Journal of cell biology* 173(1):19-26.

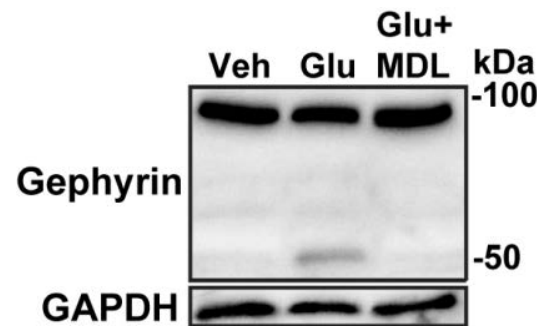
Supplementary Data



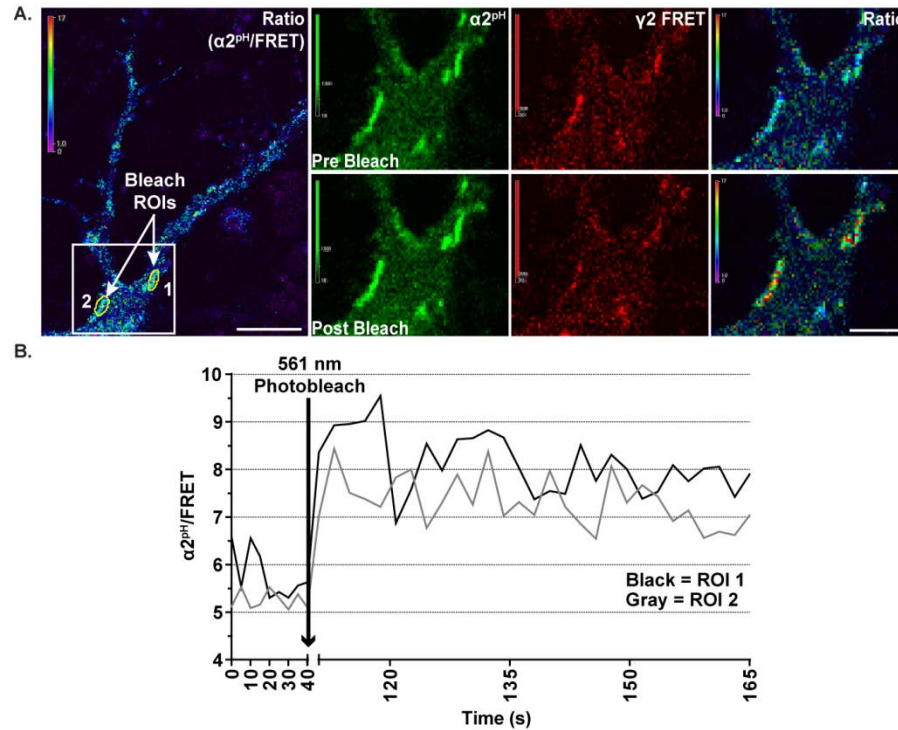
Supplementary Figure 1. Membrane fractionation characterization. DIV 16 neurons were lysed with fractionation buffer and separated by centrifugation. Western blot analysis shows the intracellular trafficking protein EEA1 is only found in cytosolic and total fractions. Conversely, the plasma membrane protein KIR 3.2 is highly enriched in the membrane fraction.



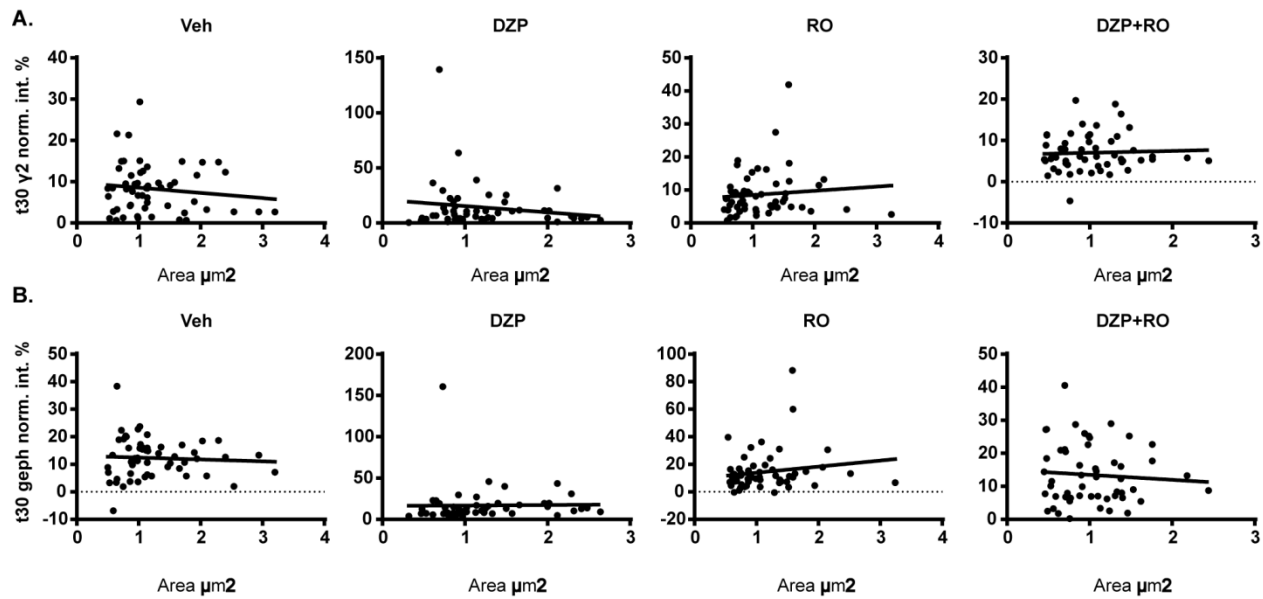
Supplementary Figure 2. Validation of denaturing conditions for $\gamma 2$ subunit isolation from receptor complex. HEK293 cells were transfected with GABA_AR subunit DNA $\gamma 2^{\text{pH}}$ FAP, $\beta 3$ -RFP and $\alpha 2$ -HA in a 1:1:1 ratio. Cells were lysed either standard control RIPA conditions (Con) or denaturing conditions (Den) using 1% SDS and 20 min exposure to 50°C heat. Lysates were immunoprecipitated with control IgG or rabbit GFP-antibody. Blots probed with chicken GFP and mouse RFP antibody. Right blots are total lysate expression.



Supplementary Figure 3. Calpain-1 dependent gephyrin cleavage upon glutamate stimulation. DIV 16 neurons were treated with vehicle or 100 μ M glutamate for 30min in HBS +/- 10 μ M calpain-1 inhibitor MDL-28170 (MDL). Neurons were then returned to conditioned media for 1.5 h prior to lysis. MDL-28170 treated neurons were in presence of inhibitor throughout experiment. Calpain-1 inhibition mitigates glutamate induced cleavage of gephyrin. Top band indicates full length gephyrin (95 kDa), bottom band indicates cleaved gephyrin (~50 kDa).



Supplementary Figure 4. $\alpha 2^{pH}$ and $\gamma 2^{RFP}$ participate in intermolecular FRET within GABA_AR complexes. A. FRET occurs between $\alpha 2^{pH}$ donor and $\gamma 2^{RFP}$ acceptor in DIV 15-16 cortical neurons. Time-series imaging examined pre bleach and post bleach synaptic sites after photobleaching of $\gamma 2^{RFP}$ (acceptor) with 561 nm laser for 1 minute. B. Acceptor $\gamma 2^{RFP}$ bleaching results in elevated $\alpha 2^{pH}$ fluorescence, evidencing previous FRET between fluorophores.



Supplementary Figure 5. Synapse cluster size does not correlate with the rate of fluorescence recovery of gephyrin and $\gamma 2$. The rate of $\gamma 2^{\text{pH}}$ -FAP (A.) and RFP-gephyrin (B.) fluorescence recovery rate at 30 min post-photobleaching was compared to synapse cluster area measured by correlation analysis. There was no significant correlation between fluorescence recovery rate and area across all conditions.

IN EXCEL FILE

Dataset 1. Proteins Identified by Label-Free Mass Spectrometry and Spectral Counts.

Identification criteria were: minimum of two peptides; 96% peptide threshold; 1% FDR; 99% protein threshold; identified in at least 3 samples overall or identified 2 of 3 times in a specific treatment group; demonstrated at least 3:1 enrichment over IgG control across at least 3 samples overall.